Geochemical identification of episodes of gold mineralisation in the Barberton Greenstone Belt, South Africa.

Altigani, MAH, Merkle, RKW and Dixon, R.D*.

* Department of Geology - University of Pretoria - Private Bag X20 – Hatfield – Pretoria – 0028- Republic of South Africa. roger.dixon@up.ac.za

Key words: Barberton, gold, hydrothermal, halogen, mineralisation.

Abstract

The morphology and mineral chemistry of gold and associated sulphides at Sheba, Fairview, and New Consort gold mines in the Barberton Greenstone Belt (BGB) identify two main types of mineralization. The first type occurs associated with sulphides (mainly pyrite), either as inclusions (10-30 μm) or as sub-microscopic gold. The second gold type consists of large gold grains (≥ 100μm) within the silicates (mostly quartz).

LA-ICP-MS studies reveal that some gold and associated sulphide grains contain high values of Cl, Br, Na, and I. The elemental relationships reflect the different chemistry and precipitation processes of possible source fluids, and identify several episodes of mineralisation in the study area, one of them formed due to a boiling process in a supercritical hydrothermal environment. This paper reports on the compositional characteristics of these gold grains, the significance of the halogen contents, and the implications for possible sources of the gold and associated sulphides.

1. Introduction

The Barberton Greenstone Belt (BGB) of the Kaapvaal Craton, South Africa (Fig. 1), is one of the oldest granite-greenstone belts in the world (Anhaeusser, , 1976, 1986; van Kranendonk *et al.*, 2009; van Kranendonk 2011), and one of the most studied Early Archaean greenstone belts worldwide (Anhaeusser, 1976, 1986; Brandl *et al.*, 2006; De Wit *et al*., 2011; van Kranendonk 2011). It is also one of the most important gold producing terrains in South Africa (Ward, 1995, 1999; Goldfarb *et al.*, 2001; Brandl *et al*., 2006), with gold production starting in the late 19th century. More than 350 gold deposits have been reported in the BGB, with more than 85% of the approximately 345 tonnes of gold produced coming from the Sheba, Fairview, and New Consort mines between 1884 to 1995 (Anhaeusser, 1976, 1986; Ward, 1999; Dirks *et al*., 2009). These three mines have a continued production of ~ 2.9 t of gold annually (Pan African Resources, 2015).

Situated in the northern terrane of the BGB, in fairly close proximity, the Fairview, Sheba and New Consort mines show very distinct characteristics (controls and conditions of mineralisation) (Dziggel *et al.*, 2006; Otto *et al*., 2007; Dziggel *et al*., 2010; Munyai *et al*, 2011; Agangi *et al*., 2014). The regional geology and structural evolution of the BGB is complex, as reflected in the extensive literature, which makes unravelling the sequence of events leading to the timing and mode of emplacement of the gold mineralisation complicated. The gold distribution in the BGB is structurally controlled (Dirks *et al*., 2009), and recent work has shown that the main phase of gold

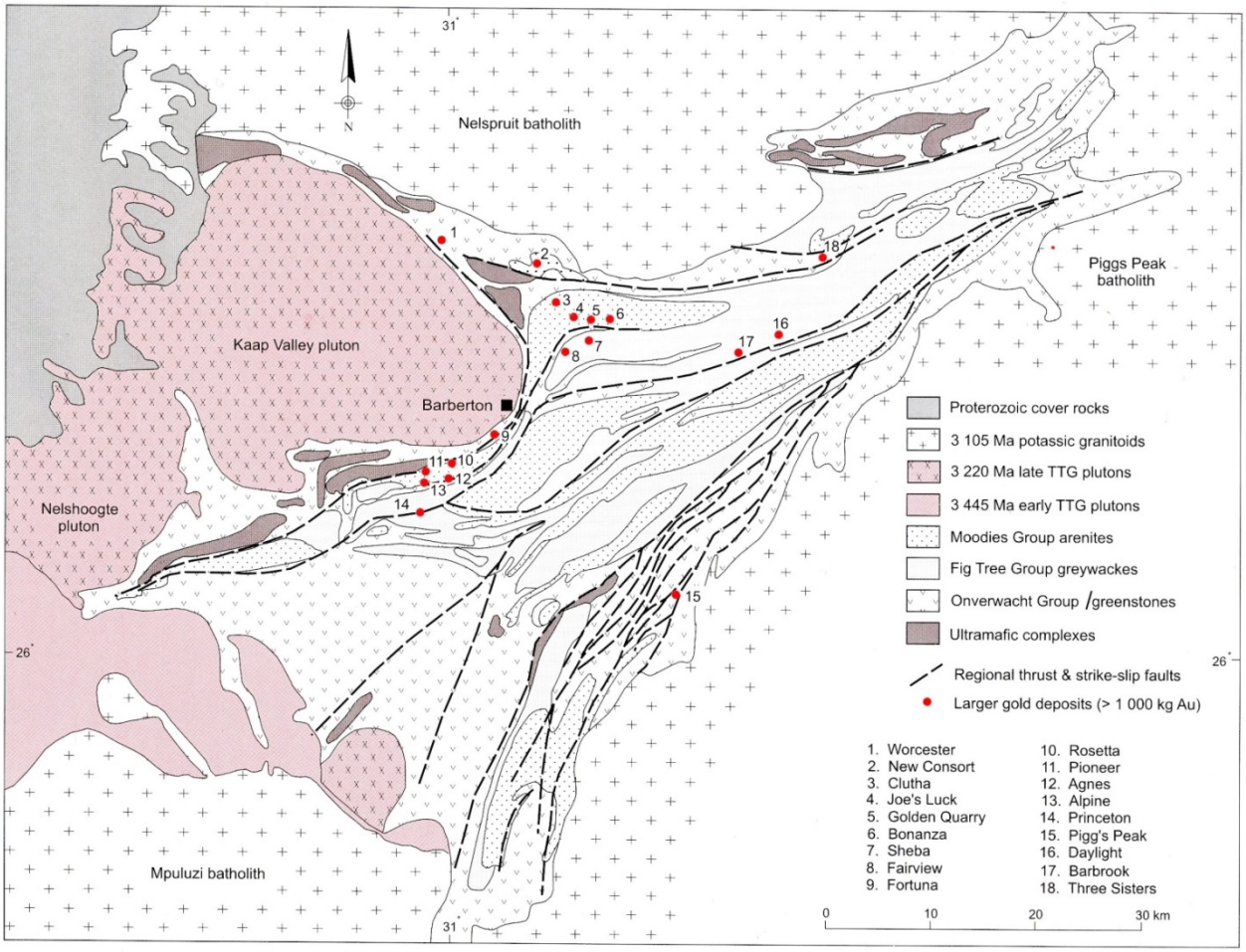

Figure 1. Simplified geology of the Barberton Greenstone Belt (after Ward & Wilson, 1998).

mineralisation in the BGB was controlled by pre-existing faults and fractures, and postdates the main structural and metamorphic episodes (Dziggel *et al*. 2010; Munyai *et al*. 2011; Dirks *et al* 2013). Dirks *et al.* (2013) proposed that the principal stage of gold enrichment in the BGB occurred after tectonic and thermal stabilisation of the Kaapvaal Craton, suggesting that brittle–ductile shear zones allowed mineralising fluids to exist during cratonic extension. Similarly, Micklethwaite & Cox (2004) have shown that the lode gold deposits in the Kalgoorlie terrane, Western Australia, in the Archean greenstone sequence of the Yilgarn craton, were the result of episodes of focused fluid flow through a pre-existing high-permeability network over extended periods.

For this investigation the mineralised assemblages, especially those containing gold, were looked at with the aim of identifying chemical clues to link gold mineralisation parageneses to possible modes of formation. Previous studies which focussed on the origin of the mineralisation based on chemistry of the ore minerals did not look at the chemistry of the gold, but rather of the associated mineral assemblages (e.g. De Villiers, 1957; Saager & Koppel, 1976; Cabri *et al*., 1989; Otto *et al*., 2007; Agangi *et al*., 2014).

Analyses by Warren & Thompson (1944) and Steele & Carlton (1961) of some gold grains from various mines in the BGB showed gold with both high and low Ag contents, in addition to trace amounts of other elements. Warren & Thompson (1944) found that differences in gold composition were related to metallogenetic zones rather than to the type of deposit. Gay (1963) reviewed gold compositions from the literature of gold around the world, including the BGB, in order to identify the genetic type of the mineralisation. He then looked at gold from Zwartkoppie Reef at Sheba mine (Gay, 1964) and came to the conclusion that there were two episodes of gold mineralisation, echoing de Villiers (1957) finding that free gold occurred late in the paragenetic sequence, except where it was enclosed in arsenopyrite. These analyses, however, were of handpicked gold grains which had been separated out of the ore, and melted together (Gay, 1964), so grains of different compositions from a single sample could have been combined.

Our study looked at the composition of individual sulphide and gold grains from the Sheba, Fairview and New Consort gold mines from the BGB (Fig. 2), as determined by EMPA and LA-ICP-MS. It evaluates the contribution that chemical variation of ore minerals has in clarifying the events that led to the gold mineralisation.

.

2. Analytical procedures

In order to assess the variability of mineral compositions, the major and trace elements were measured, respectively using a CAMECA SX-100 electron microprobe (University of Pretoria) and Laser Ablation ICP-MS (Forensic Science Laboratory, Pretoria). The measurements were performed on epoxy mounted polished sections and are presented in Table 1. Quantitative phase analysis (XRD) was performed to obtain weight percentages of minerals in the various samples.

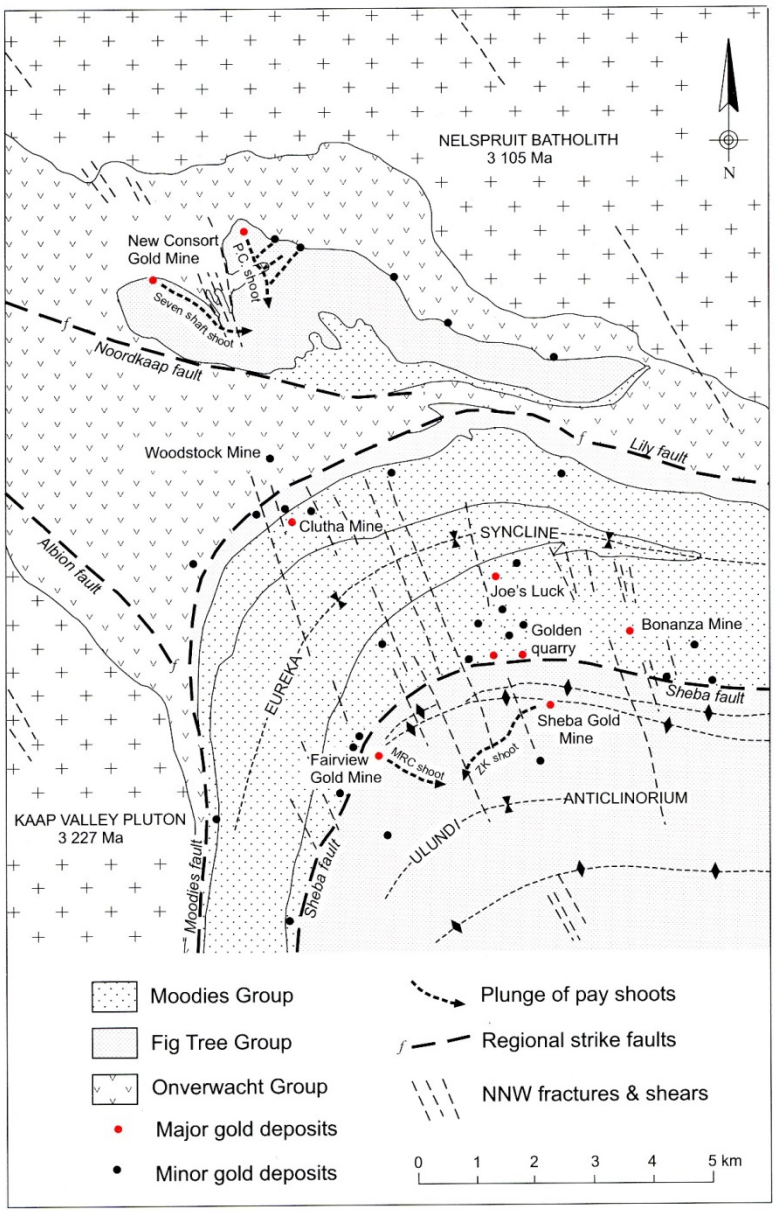

Figure 2: Detailed geology of the New Consort-Fairview-Sheba area (after Ward & Wilson, 1998).

	Gold						Pyrite						Arsenopyrite					
	Type 1			Type 2			Type 1			Type 2			Type 1			Type 2		
	Sheba	Fairview	New Consort	Sheba	Fairview	New Consort	Sheba	Fairview	New Consort	Sheba	Fairview	New Consort	Sheba	Fairview	New Consort	Sheba	Fairview	New Consort
S	-	-	(0-0.08)	(0.05-0.01)	-	(0-1.29)	(51.2-53.3)	(50.1-53.8)	-	(52.16-53.43)	(50.1-53.8)	-	(18.03-18.97)	(16.5-24.4)	(17.46-19.37)	(19.1-20.3)	(18.48-24)	(21.2-22.5)
Fe	-	-	(0-2.72)	(0.37-0.24)	-	(0-1.55)	(45.2-46.4)	(44.1-47.7)	-	(46.2-46.95)	(43.7-47.5)	-	(32.62-33.33)	(29-35.9)	(30.53-33.77)	(33.3-34.4)	(30.48-36.4)	(34.7-36.3)
As	-	-	(0-0)	(0-0)	-	(0-0.83)	(0.4-2.13)	(0-0.48)	-	(0-0.95)	(0-5.1)	-	(47-9-50.04)	(38.9-50.4)	(47.23-49.08)	(45.5-46.9)	(38.1-44.7)	(40.8-43.4)
Co	-	-	(0-0.04)	(0-0)	-	(0-0.05)	(0-0.21)	(0-0.49)	-	(0-0)	(0-0.2)	-	(0-0.11)	(0-0.69)	(0-1.76)	(0-0)	(0-0.01)	(0-0)
Ni	-	-	(0-0.11)	(0-0.01)	-	(0-0.07)	(0.19-1.03)	(0-1.1)	-	(0.01-0.39)	(0-1.02)	-	(0.37-0.71)	(0-3.25)	(0-0.19)	(0.02-0.33)	(0-0.5)	(0-0.03)
Cu	-	-	(0.39-1.31)	(0.07-0.09)	-	(0-0.15)	(0-0-03)	(0-1.98)	-	(0-0.03)	(0-0.6)	-	(0-0.04)	(0-0.06)	(0-0.04)	(0-0.03)	(0-0.08)	(0-0.04)
Zn	-	-	(0-0.06)	(0-0)	-	(0-0.06)	(0-0.03)	(0-0.54)	-	(0-0.03)	(0-1.04)	-	(0-0.04)	(0-0.05)	(0-0.04)	(0-0.03)	(0-0.06)	(0-0.013)
Pd	-	-	(0-0.06)	(0-0)	-	(0-0.14)	(0-0.13)	(0-0.14)	-	(0-0.07)	(0-0.12)	-	(0-011)	(0-0.15)	(0-0.03)	(0-0.13)	(0-0.12)	(0-0.1)
Ag	-	-	(2.09-4.32)	(3.91-3.89)	-	(3.66-10.61)	(0-0.06)	(0-0.19)	-	(0-0.05)	(0-0.13)	-	(0-0.05)	(0-0.1)	(0-0.05)	(0-0.03)	(0-0.08)	(0-0)
Cd	-	-	(0-0.18)	(0-0.06)	-	(0-0.16)	(0-0.07)	(0-0.12)	-	(0-0.08)	(0-0.1)	-	(0-0.09)	(0-0.15)	(0-0.03)	(0-0.09)	(0-0.11)	(0-0.01)
Sb	-	-	(0-0.1)	(0-0)	–	(0-0.05)	(1-0)	(0-0)	-	(0-0)	(0-0)	-	(0-0)	(0-0)	(0-0)	(0-0)	(0-0)	(0-0)
Au	-	-	(92.31-96.76)	(96.24-95.53)	-	(85.05-96.36)	(0-0.05)	(0-1.7)	-	(0-0.11)	(0-0.18)	-	(0-0.22)	(0-0.4)	(0-0.11)	(0-0.1)	(0-0.32)	(0-0.2)
Hg	-	-	(0-0)	(0-0)	–	(0-0)	(0-0.12)	(0-0.27)	-	(0-0.14)	(0-0.31)	-	(0-018)	(0-0.24)	(0-0.14)	(0-0.1)	(0-0.173)	(0-0.16)
Pb	-	-	(0-0.21)	((0.00-0.29)	-	(0-0.26)	(0-0)	(0-1.5)	-	(0-0)	(0-0.01)	-	(0-0.16)	(0-0.17)	(0-0.22)	(0-0.16)	(0-0.46)	(0-0.08)
Bi	-	-	(0-0)	(0-0)	–	(0-0.03)	(0-0.22)	(0-0.37)	-	(0-0.25)	(0-0.35)	-	(0-0.71)	(0-0.77)	(0.14-0.54)	(0.2-0.5)	(0-0.78)	(0.2-0.51)
Mn	-	-	(0-0)	(0-0)	–	(0-0)	(0-0.02)	(0-0.04)	-	(0-0.03)	(0-0.03)	-	(0-0.03)	(0-0.05)	(0-0.04)	(0-0.02)	(0-0.04)	(0.01-0.05)

Table 1: Minimum and maximum values of the EMPA analyses (wt. %) of gold, pyrite, and arsenopyrite from the studied mines (Sheba, Fairview, and New Consort).

2.1 Electron probe microanalysis (EMPA)

Imaging and elemental analysis were performed using an electron microprobe in the gold and sulphide ores from the Sheba, the Fairview, and the New Consort mines. The spectra were processed by ZAF corrections. Analysis of the samples was performed with an accelerating voltage of 20 kV, a current of 20 nano ampere (nA), and a focused spot (<1 µm diameter). Counting times were 10 seconds for all elements. The standards used for calibration were as follows: albite (Si, Na, K), MgO (Mg), Al_2O_3 (Al), topaz (F), apatite (P), andradite (Ca), orthoclase (K), Fe_2O_3 (Fe), vanadinite (Cl) and MnTi standard (Mn, Ti).

2.2 Laser ablation-inductively coupled plasma-mass spectrometry (LA-ICP-MS)

Electron-microprobe work by Hayward *et al*. (2005) on Witwatersrand gold grains and Merkle *et al*. (2008) on gold grains from the Merensky Reef shows that gold grains are heterogeneous and may contain inclusions, so bulk analyses have limited potential in working out genetic relationships based on elemental distributions. Accordingly, mineral grains were analysed by LA-ICP-MS in order to determine elemental distribution within the grains.

The trace elements were measured using an Agilent 7500 CX inductively coupled plasma mass spectrometer coupled to a New Wave 213 nm laser. Ablation was performed in He, and the gas then mixed with Ar prior to delivery to the MS. Between run normalisation was achieved using the bracketing technique over an NIST 612 glass (Pearce *et al*., 1997) analyzed every 20 spots.

For spot analyses, the samples were ablated using a spot size and depth of 25 µm, with an energy of 5 J/cm2 and a 4 Hz repetition rate, for 45 seconds. The resolution of the laser spot is not as small as that which is achievable by an electron microprobe, but elemental concentrations of a wide range of elements down to ppb levels are possible. The LA-ICP-MS results are not quantified to standards, but expressed as count per seconds (cps). Some grains were mapped on a grid pattern, with continuous ablation via successive line scans to determine elemental distributions. A laser spot size of 10 µm was selected, with a scan speed of 10 μms^{-1} and a sampling rate of ~0.25 s. This translates to an effective sampling area of 2.5 x 10 µm. The utility of this methodology in increasing the resolution compared to spot analyses has been discussed by Sanborn and Telmer (2003), who showed that LA-ICP-MS line scans could produce similar or better information about elemental distribution in a heterogeneous solid than spot analysis.

3. Results3.1 Samples

As the aim of this study was a better understanding of the origin of the gold and its formation, 20 samples of gold-rich ores were selected from the three mines for petrography and elemental analysis. From the Sheba Mine four samples were collected from the Zwartkoppie Reef, the Main Reef Complex, Drummond Reef, and Commitment

Reef. From Fairview Mine, 12 samples were collected from the Commitment Main Reef (CMR), MRT and Main Reef Complex (MRC). The four samples from the New Consort Mine came from the Consort Contact Reef.

3.2 Sample description

Sheba Mine

At Sheba Mine three stages of ore mineralisation were identified. These stages are identified by the sulphide mineral assemblage, the appearance and associations of the gold, and the chemical variation within all the ore mineral phases. The main minerals (pyrite, arsenopyrite, and gold) show two distinct generations based on textural associations and chemical composition. These are referred to as Type 1 and Type 2. Three stages of mineralisation are observed which are characterised by the textural and mineral associations with the gold. These are referred to as Stage 1, Stage 2 and Stage 3. Stage 1, based on petrography, has been identifed as the first stage of mineralisation, followed by Stage 2. These first two stages are sulphide assemblages. The third assemblage, Stage 3, is characterised by large free gold grains hosted in a mainly siliceous matrix. Previous work has identified two mineralisation types in the BGB, being the sulphide and silicate assemblages (Shweigart & Liebenberg, 1966), with two generations of arsenopyrite and pyrite identified (Steyn, 1976; Agangi *et al*., 2014). Schouwstra (1985) showed that the gold mineralisation in the MRC was structurally controlled and of hydrothermal origin.

Stage 1:

The main host rocks of this type at Sheba are metapelites and greywackes, characterised by the presence of biotite, garnet, muscovite, dolomite, chlorite, and quartz, indicative for low-grade metamorphism. The ore-mineral assemblage consists of pyrite (Type 1, cores), arsenopyrite (Type 1), anhedral chalcopyrite, porous pyrrhotite and visible gold Type 1.

The pyrite Type 1 (Fig. 3) in this assemblage is porous, displays irregular shapes and zonation features, and hosts inclusions of arsenopyrite, pyrrhotite, chalcopyrite, minor sphalerite, silicates, and infrequently gold. Rotation and pressure shadow textures are common with this pyrite (Fig. 4a); tiny quartz and muscovite grains are located in these shadows (Fig. 4b), sometimes they form radial and fibrous textures, in other cases quartz is found as small polygons. This pyrite type occurs typically at the core of large pyrite grains and is recognized by discernable zonation.

Two generations of arsenopyrite (Figs. 5a,b,c, 6) can be distinguished in this mine, with the relatively older Type 1 associated with porous pyrrhotite and gold Type 1. This arsenopyrite forms irregularly shaped grains with oscillatory growth zones, and is found as large accumulations of small grains (Fig 5a). Zoning and intergrowth textures (particularly with pyrrhotite) are common, and it hosts gold inclusions (Fig. 5c).

Anhedral chalcopyrite forms irregular grain shapes, found inside pyrite, and as fracture-filling veinlet and stringers in both pyrrhotite and arsenopyrite. Porous pyrrhotite forms large grains adjacent to arsenopyrite, and is also found as small inclusions inside pyrite.

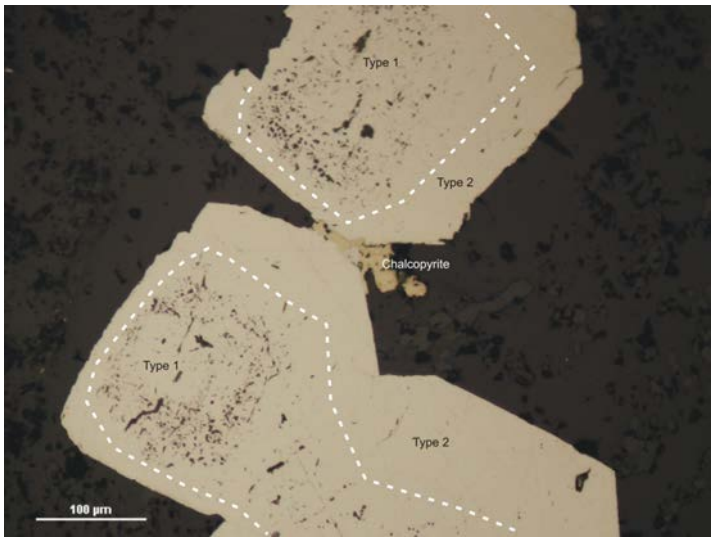

Figure 3: Pyrite grains from Sheba mine. Type 1 core (porous) and Type 2 rim (massive).

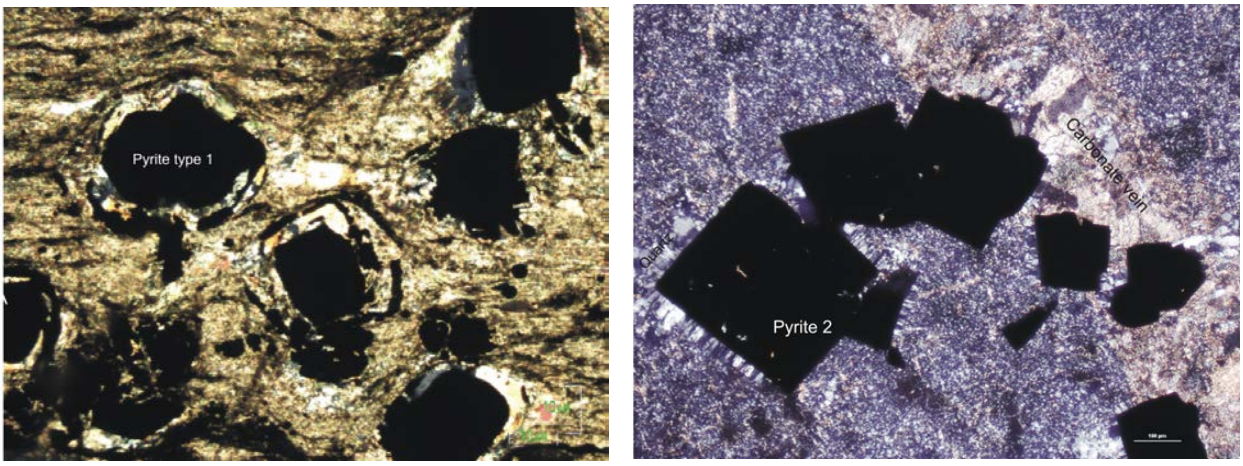

Figure 4: A (left): Pyrite Type 1 in metapelite, sample 125941, section B, Sheba Mine, showing rotation of the pyrite grains. B (right): Pyrite Type 2 in arenaceous rocks, FSC-307917, Sheba Mine, located close to a carbonate vein, with fibrous quartz located in the pressure shadows.

Gold Type 1 is commonly found as small inclusions inside and between pyrite Type 1, porous pyrrhotite and arsenopyrite Type 1 (Figs 3,4).

Stage 2:

The main host lithologies of this stage are arkoses and arenaceous rocks. These rocks consist of quartz (50 wt %), muscovite, biotite, carbonate minerals, and rare garnet.

The sulphides here include pyrite Type 2, arsenopyrite Type 2, euhedral chalcopyrite and massive pyrrhotite. Pyrite Type 2 is massive (Fig. 3), well developed, euhedral, and relatively younger, and is found overgrown on the pyrite Type 1, and as well-developed crystals. This pyrite is homogenous and shows no zonation or inclusions when using optical microscopy or back-scattered electron imaging. Nevertheless, the use of LA-ICP-MS mapping revealed micro-zoning and very minute inclusions in this type (Figs 6,7). No visible gold was observed in this assemblage, and there is a lot less arsenopyrite present compared to the Stage 1 assemblage.

Stage 3:

This mineralization stage contains gold Type 2 (Fig. 8) within quartz veins and siliceous assemblages (quartz, mica, carbonates). It occurs as large irregular grains within the silicates as free gold.

Fairview Mine

The Fairview rocks were originally arenites, interlayered with thin layers of impure (micaceous) sandstones and basic volcanics (De Vries *et al*., 2006; Hessler & Lowe, 2006; Stiegler *et al*., 2010), and consist mainly of quartz, calcite, dolomite, and muscovite. This mineral association is indicative of low-grade greenschist facies metamorphism (Miyashiro, 1973; Stiegler *et al*., 2010).

In the metapelite sample from the CMR (FSC-308168), biotite, actinolite, plagioclase, hornblende and chlorite are the dominant minerals (Fig. 9), with the biotite (3.2-15wt. %) and actinolite (up to 25.5wt. %.) forming a radial fibrous texture. Albite shows some deformation microstructures, such as tapered and conjugate lamellae. Muscovite, quartz, sphene, epidote group minerals, and chlorite are present in lesser amounts. The arkoses (Fig. 10) comprise mainly of quartz (35-67.5 wt. %), in four different habits: (1) the first is angular and fragmented quartz. (2) The second is medium to coarse-grained deformed crystals, which show kidney-shaped and augen deformational micro-textures. (3) The third type is represented by small post-tectonic polygons that are located in the pressure shadows of the sulphides (mainly pyrite), and (4) rounded to sub-rounded quartz represents the fourth type (Fig. 10). Muscovite (fuchsite) is sub-dominant, associated with small calcite veins, ranging from 28.2 wt. % to 42.2 wt. % of these rocks. Muscovite is also found as radial lepidoblastic laths, and small sheets situated in pressure shadows of the large quartz and sulphide porphyroblasts. Dolomite is a common secondary component within these rocks; epidote, graphite, and chlorite are rarely found representing the accessory minerals. Greywackes, generated from impure calcareous sandstones, are rich in augen quartz (32-51.9 wt. %). Carbonate

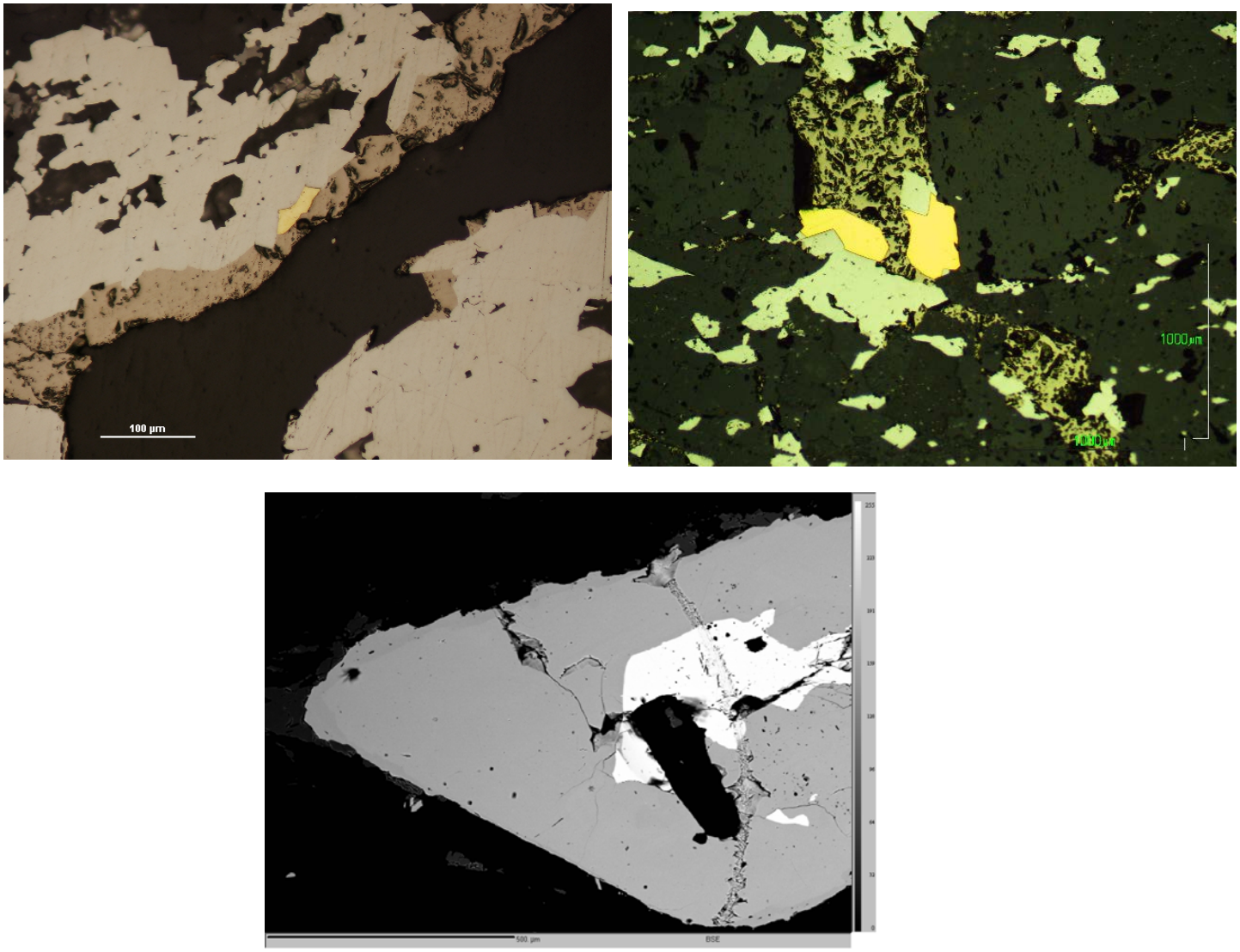

Figure 5: A (top left) & B (top right) Gold Type 1 (yellow) from Sheba Mine, associate porous pyrrhotite (pale brown), and arsenopyrite Type 1 (light). C (bottom) arsenopyrite Type 1 (light grey) contains euhedral gold grains (white). Sample 125941, section A1, Sheba Mine.

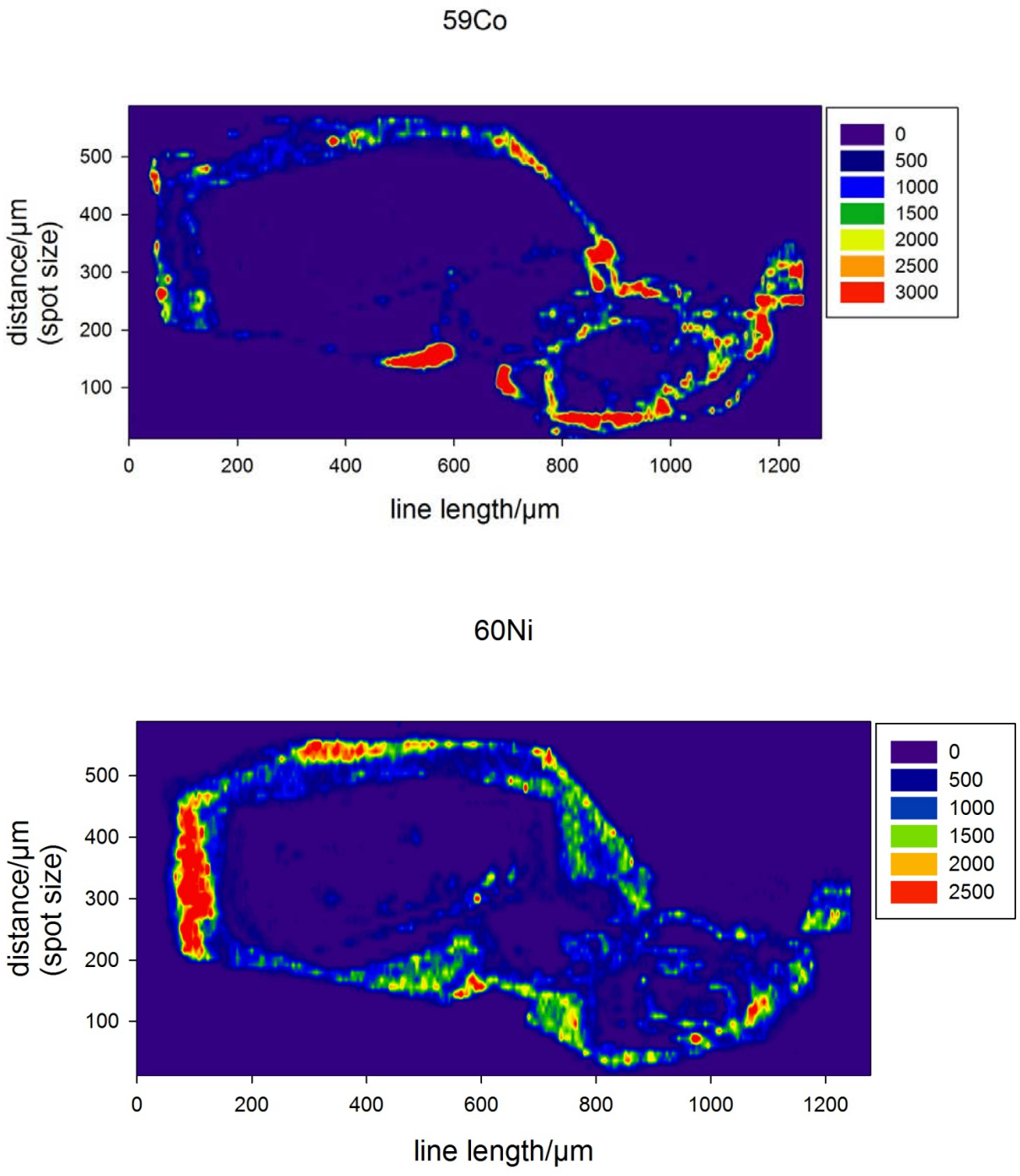

Figure 6: A composite pyrite grain from Sheba showing the distribution of Co and Ni. It can be seen that the grain consists of anhedral Type 1 grains, which have been included into the growth of a euhedral Type 2. What is also obvious is that the behaviour of Co and Ni in the pyrite structure is not linked, and appears antipathetic.

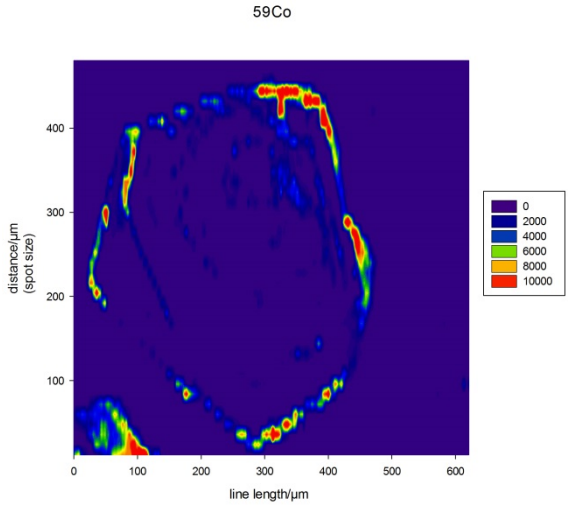

Figure 7. LA-ICP-MS maps of a pyrite grain from Sheba, showing an anhedral Type 1 (core) and a euhedral Type 2 rim. It can be clearly seen that the gold is associated with the Type 1 pyrite, together with such elements as Pb, Sb and Cu. Gold is not associated with the Type 2 pyrite, which shows distinct zonation of the Ni and As. Co is not correlated with the Ni and Zn, and appears as one of the last elements to be included into the pyrite structure.

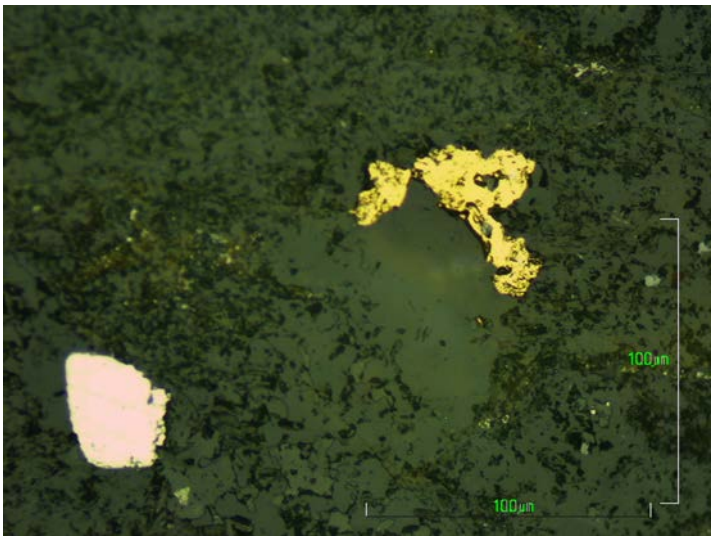

Figure 8: Irregular gold Type 2 (yellow) of Stage 3 attached to a quartz grain, from sample FSC-307917, Sheba Mine. Arsenopyrite Type 2 is in the lower left corner.

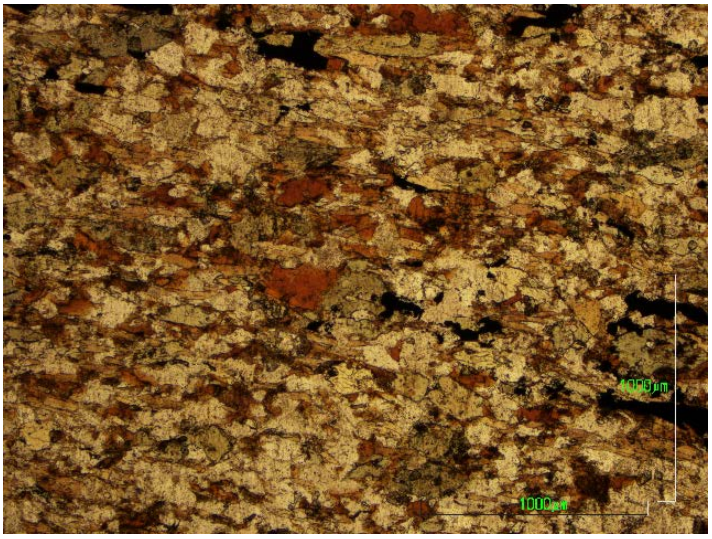

Figure 9: Metapelite from Fairview Mine: biotite (brown), actinolite (pale green), quartz (white). Sample FSC-308168.

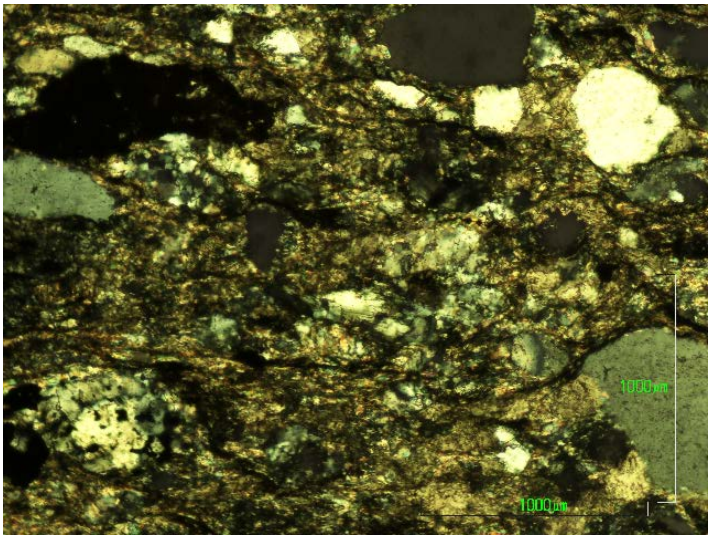

Figure 10: Arkose from Fairview Mine: poorly sorted, different shapes and sizes of quartz grains, with a carbonaceous groundmass. Sample RBB-87913.

minerals are represented by calcite and dolomite (16 wt. %). Green muscovite (fuchsite**)** (26.5-50 wt. %) follows the foliation planes, and is situated at pressure shadows. In some cases, it is found as radial large patches.

Fairview Gold Mine is located along the central and southern sections of the Eureka and Ulundi Synclines (Fig. 2) (Otto *et al*., 2007; Dziggel *et al*., 2007), which are separated by the Sheba Fault, bound to the north by the Lily Fault and to the south by the Barbrook Fault (Otto *et al*., 2007; Dziggel *et al*., 2007). These synclinorium structures were refolded with north-west fractures axes, resulting in the development of fractures (structural porosity), which are considered to be the host structures of the gold mineralization at Fairview (Dziggel *et al*., 2007), which is mainly in quartz-carbonate veins (Hofmann & Harris, 2008).

Previous work has identified two types of gold mineralization at the Fairview Mine – sulphide reefs and quartz reefs. The sulphide reefs consist of disseminated to massive sulphides, situated at concordant and discordant structures in the greywackes and shales. Fractures in these rocks were formed due to the tangential shears, which initiated during the major folding events (Dziggel *et al*., 2007; Lana *et al*., 2010; Lana *et al*., 2011). The sulphide reefs range from 2 cm up to 2 m in width, and extend approximately 500 m along strike (Otto *et al*., 2007; Dziggel *et al*., 2007). The principal associated sulphides are pyrite and arsenopyrite, with minor chalcopyrite, sphalerite, pyrrhotite, and gersdorffite (Heubeck *et al*., 1993). Calcite, quartz, and sericite are the most important gangue minerals. Heubeck *et al*. (1993) estimate that around 50% of the gold is found in pyrite, 20% in arsenopyrite and associated minerals, and the remainder as free gold. This type is comparable to our gold Type 1, occurring in mineralisation Stage 1.

The second type of the gold mineralization is in quartz reefs located perpendicular to the strike of the host rocks and the Sheba Fault. These reefs contain only a small amount of pyrite or arsenopyrite, and often contain visible, disseminated films and plates of gold (Wiggett *et al*., 1986; Heubeck *et al*., 1993; Otto *et al*., 2007), comparable to our gold Type 2 occurring in mineralisation Stage 3.

Stage 1:

This stage is typified by the presence of of pyrite Type 1 with arsenopyrite Type 1, porous pyrrhotite, anhedral chalcopyrite and gold Type 1, with minor loellingite, nickeline, gersdorffite and sphalerite. These ore-minerals are hosted in metapelites, arkoses, and greywackes.

Pyrite Type 1 (Fig. 11) is densely included by arsenopyrite Type 1, porous pyrrhotite, anhedral chalcopyrite (Fig. 12), and gold Type 1. It commonly displays a variety of microtextures, such as zoning and atoll textures (Figs 13a,b). Arsenopyrite Type 1 forms irregular gains with twin lamellae and zonation textures, long, rhombic, and separate glomeroblasts, occasionally sub-rounded (Fig. 14). Anhedral chalcopyrite at Fairview is found as kinked bands inside the pyrite Type 1. The chalcopyrite forms zoned and gradational rims with porous pyrrhotite, indicating growth zones, or repeated fluid cycles, possibly indicating that the chalcopyrite formed due to replacement of the pyrrhotite in the presence of aqueous copper (Elliot & Watling, 2011). Pyrrhotite is dominant in all the Fairview Mine rocks, found in large (up to 5mm) patch-like aggregates, usually occurring adjacent to

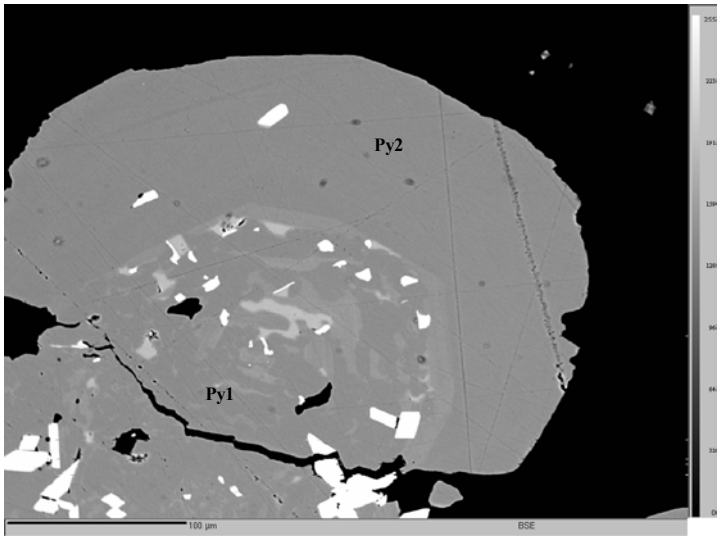

Figure 11: Pyrite Type 1 core (contains inclusions of pyrrhotite, and As-rich zones) surrounded by pyrite Type 2 rim from Fairview. The arsenopyrite is Type 2 (bright)

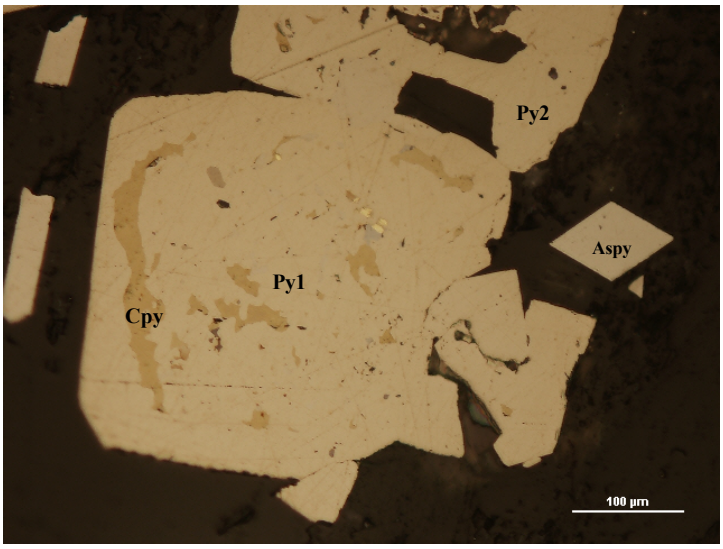

Figure 12: Fairview pyrite Type 2 (rim) surrounding pyrite Type 1 (core), which enclosed by gold Type 1 (yellow), chalcopyrite (Cpy), pyrrhotite (greyish), and associated arsenopyrite Type 2 (Aspy).

Table 2: Correlation between the ore mineralogy in the three studied mines.

Mine/ Mineral	Gold	Pyrite	Arsenopyrite	Chalcopyrite	Pyrrhotite
Sheba	Type 1 within sulphides (pyrite), as small inclusions and invisible phases. Type 2 found in silicates (quartz, carbonate)	Type 1 pyrite is often found as cores to pyrite grains, associated with Type 1 arsenopyrite, porous pyrrhotite, anhedral chalcopyrite, and Type 1 gold. Pyrite Type 2 often occurs as rims to zoned grains and as euhedral grains, together with arsenopyrite Type 2, massive pyrrhotite, euhedral chalcopyrite, sphalerite, löllingite, gersdorffite, nickeline, and gold Type 2.	Type 1: iregular, zoned, associated with pyrite Type 1, porous pyrrhotite, anhedral chalcopyrite. Type 2: euhedral, associated with pyrite Type 2, minor sphalerite	Type 1 anhedral, minor, small inclusion inside and between pyrite Type 1. With porous pyrrhotite, arsenopyrite Type 1, gold Type 1 Type 2 euhedral, asociated with pyrite Type 2,	Type 1 porous. Minor small grains inside the pyrite, associated with chalcopyrite Type 1, arsenopyrite type1, and gold Type 1. Type 2 large massive grains
Fairview	Type 1 within sulphides as small inclusions and invisible phases accumulated inside pyrite Type 1, arsenopyrite Type 2. Type 2 found within silicates (quartz, micas, ±carbonate).	Type 1 pyrite with arsenopyrite Type 1, porous pyrrhotite, anhedral chalcopyrite, and gold Type 1. Type 2 pyrite, arsenopyrite Type 2, massive pyrrhotite, euhedral chalcopyrite, sphalerite, löllingite, gersdorffite, nickeline, and gold Type 2	Type 1: iregular, zoned, hetergenous associated with pyrite Type 1, porous pyrrhotite, and tiny gold Type 1 with minor löllingite and gersdorffite. Type 2: euhedral, associated with pyrite Type 2, gold Type 2,	Type 1 - anhedral, and rare Type 2 as euhedral grains associated with pyrite Type 2 and arsenopyrite Type 2.	Type 1 porous. Small grains inside the pyrite Type 1, large patches associated with anhedral chalcopyrite, arsenopyrite Type 1 and gold Type 1. Type 2 large massive associated with arsenopyrite 2
New Consort	Type 1 found in sulphides as small inclusions and invisible phases associated with pyrrhotite, chalcopyrite and arsenopyrite. Type 2 found in silicates (quartz, carbonate, ±amphiboles)	Type 1 Very rare, associated with porous pyrrhotite, and iron oxides.	Type 1: iregular, porous pyrrhotite, sphalerite, pyrite Type 1 Type 2: associated with massive pyrrhotite, and gold Type 2 major löllingite and gersdorffite.	Type 1 Associated with porous pyrrhotite, gold Type 1, and arsenopyrite Type 1	Type 1 Stock-work, porous large patches associated with gold Type 1, anhedral chalcopyrite, and arsenopyrite Type 1. Filling interstitials of silicates.

arsenopyrite 1, anhedral chalcopyrite, and gold Type 1. Gold Type 1 is found in small, irregular, heterogeneous grains, located inside or on the periphery of sulphides (mainly pyrite Type 1), and as submicroscopic grains in arsenopyrite Type 1 (Vaughan & Kyin, 2004; Reich *et al.*, 2005; Winderbaum *et al.*, 2012), porous pyrrhotite, and anhedral chalcopyrite, as well as in larger grains varying from <10 μm to ~ 30 μm (Table 2), indicating one or more of the following modes of formation: (1) early existence of gold grains, which were over-grown or formed simultaneously with pyrite Type 1, (2) co-precipitation of gold in the structure of these sulphides, suggesting direct contribution of the ore-forming hydrothermal system rather than recrystallization effects (Economou-Eliopoulos *et al*., 2007), or (3) later auriferous hydrothermal fluids that deposited gold in fractured surfaces of the pyrite Type 1.

Stage 2:

The mineral assemblage of this stage consists of pyrite Type 2, arsenopyrite Type 2, euhedral chalcopyrite, massive pyrrhotite, and minor sphalerite, löllingite, gersdorffite and nickeline (Table 2). This stage occurs in the same rock types as that of Stage 1. Pyrite Type 2 (Figs 11,13) is younger, compact, and euhedral, often forming rims on the older pyrite Type 1. It is usually found as a separate phase, occasionally adjacent to arsenopyrite Type 2 and even less with massive pyrrhotite. The grain size of this pyrite type increases when located close to the late quartz-carbonates veins. Pyrite Type 2 rarely contains any other sulphide inclusions. Arsenopyrite Type 2 (Figs 15a,b), forms euhedral grains and is associated with pyrite Type 2, or occurs as isolated glomeroblasts within the silicates. It infrequently displays an atoll texture. No visible gold is observed in the Stage 2 assemblage.

Stage 3:

This stage was observed associated with arenites, quartzites, and rarely with arkoses. It is composed of large nuggets (>100 μm) found filling the spaces between silicates (quartz, micas) and carbonates.

New Consort mine:

Meta-volcanoclastics (komatiite tuffs) and metapelites represent the majority of the New Consort Mine rocks. They were most likely formed in back-arc basins or intra-arc basins (Raymond, 2002), and/or beneath island arcs (Miyashiro, 1973). The metamorphosed komatiites of this mine are mainly composed of biotite (up to 52.2 wt. %,). This biotite forms radial plates, suggesting hydrothermal metasomatism. A second phase of biotite was formed through the alteration of both amphiboles and garnets. Dziggel *et al*. (2007) reported Cr-muscovite + K-feldspar + plagioclase and quartz assemblage for the low-grade rocks of the New Consort Mine. Muscovite (up to 11.6 wt. %) is widespread in the New Consort Mine metapelites, occasionally formed due to the alteration of plagioclase, and is found as large augen. The muscovite layers forms micro interfolial folds, coupled with two foliation directions observed in these samples (Fig. 16), suggesting syn-tectonic shearing, which is not concordant with the primary foliation of the metapelites. Hornblende (up to 39.6 wt. %) and actinolite (up to 9.2 wt. %) are the most common amphiboles in the New Consort Mine rocks and place these rocks in the medium- to high amphibolite metamorphic facies. They are discordantly oriented to the general foliation direction, and form resistant euhedral glomeroblasts and polygonal aggregates, indicating the pre-existence of these amphiboles, before the formation of mica and replacement of former phenocrysts (probably pyroxene), and suggesting a pre-deformation existence of the

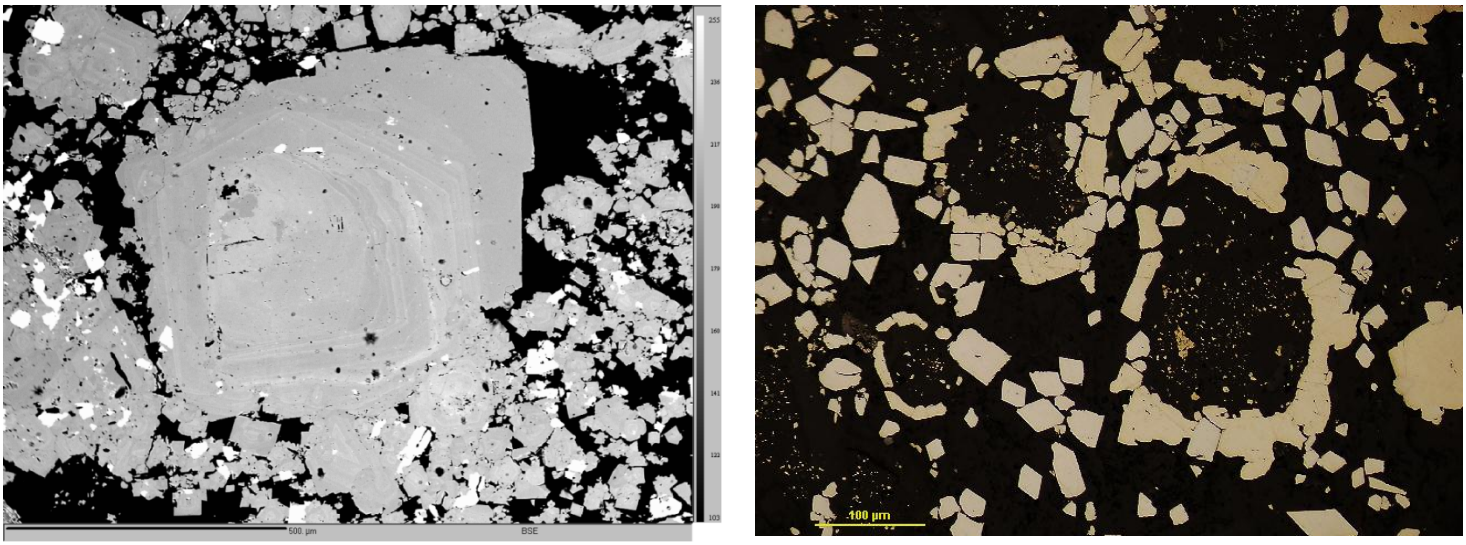

Figure 13 A (left): Pyrite Type 1 core shows heterogeneity and zoning, surrounded by pyrite Type 2 rim. B (right): Atoll pattern of arsenopyrite Type 2 and pyrite Type 2, surrounding silicates grains (quartz), which enclose small grains of pyrite Type 1 and pyrrhotite from Fairview.

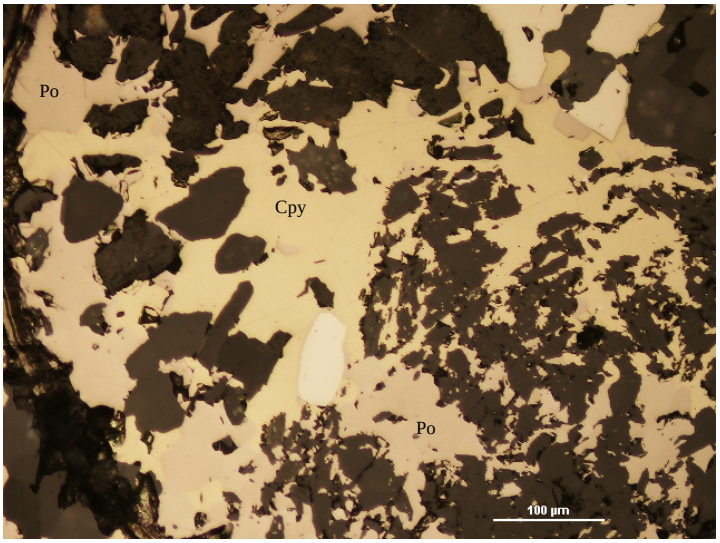

Figure 14: Arsenopyrite Type 1 (bright), associated with anhedral chalcopyrite (Cpy) and pyrrhotite (Po) from Fairview mine.

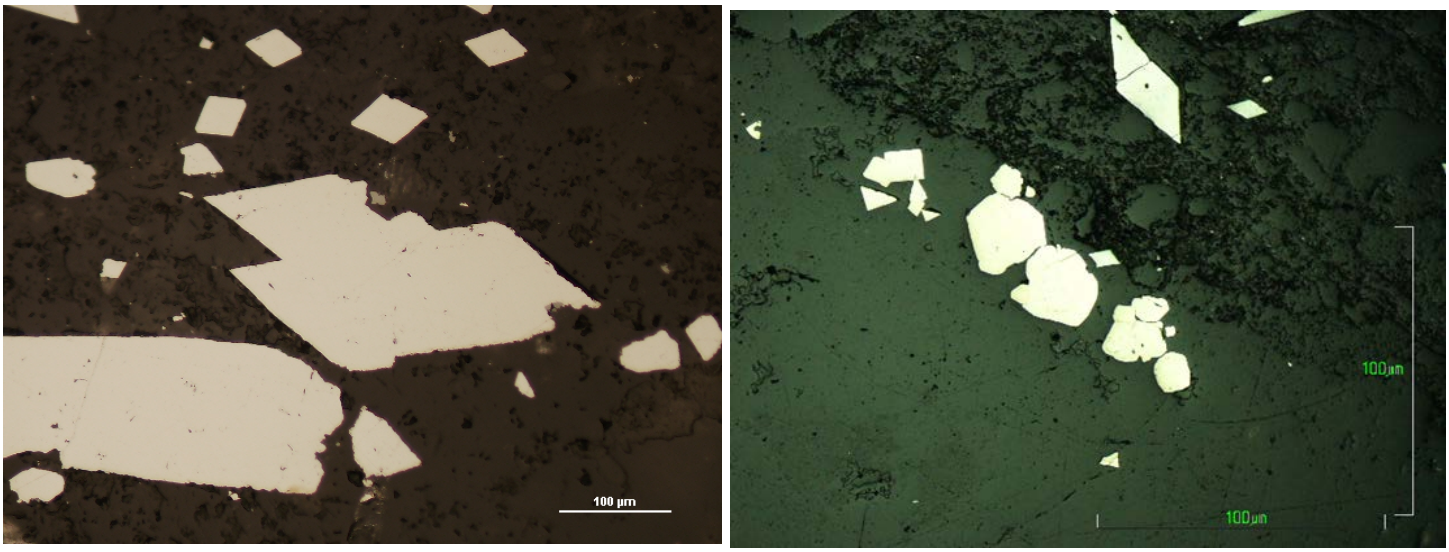

Figure 15: A (left): arsenopyrite Type 2 from Fairview mine. B (right): Stage 2: pyrite Type 2 and arsenopyrite Type 2 (euhedral), aligned along a later quartz vein, sample 125487, Fairview Mine.

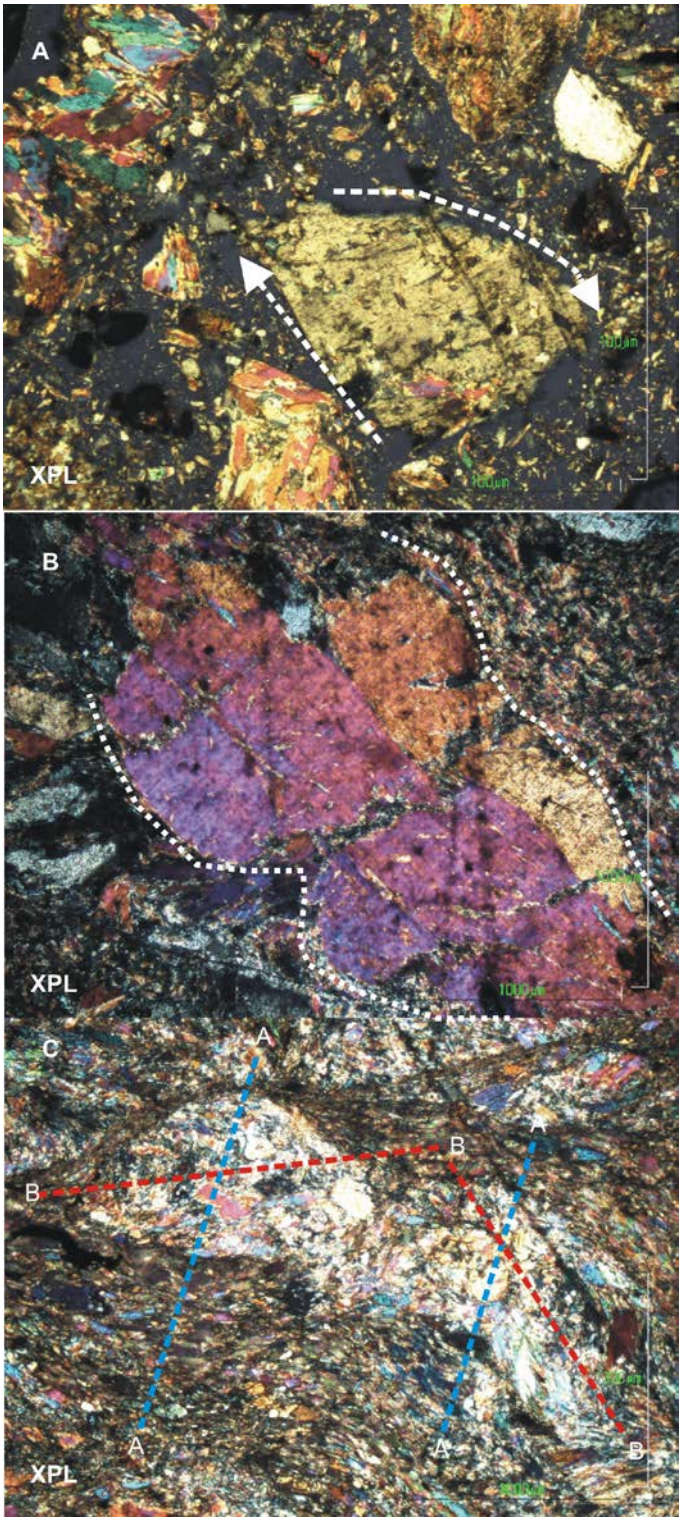

Figure 16: Transmitted light photomicrograph of New Consort Mine (A): komatiitic tuff, fragments of amphiboles, biotite, and muscovite in mylonitic glassy groundmass. (B): deformed and zoned actinolite in metapelites. (C): multiple folding phases in the muscovite, (B-B) red lines representing the older isoclinal folds, (A-A) blue line represent younger upright m-shaped folds in metapelites.

amphiboles. The alteration of hornblende to both biotite and actinolite indicates retrograde metamorphism (Dziggel *et al*., 2002). A number of other minerals are present such as quartz (5.8-23.3wt. %), albite (1.7-4.2wt. %), chloritoid (3.4-8 wt. %), graphite (up to 3.3 wt. %), and epidote (with reaction rims). Dolomite and iron-rich calcite are found in widely distributed veins associated with disseminated, well-developed sulphides.

Stage 1:

Stage 1 assemblages consist of arsenopyrite Type 1, porous pyrrhotite, anhedral chalcopyrite, gold Type 1, and very rare pyrite Type 1. Hematite and magnetite are extensively found in the ores of this mine, and loellingite, and gersdorffite are very rare. The few pyrite Type 1 grains are porous and contain inclusions of pyrrhotite and gold Type 1. Arsenopyrite Type1 (Fig. 17) forms euhedral crystals, often enclosing small gold Type 1 grains. Gold Type 1 occurs as small, sub- to euhedral grains (Fig. 17) inside the pyrite Type 1 and arsenopyrite Type 1, and also at growth boundaries of both pyrite Type 1, arsenopyrite Type 1, and löllingite. Anhedral chalcopyrite sometimes displays intergrowths with porous pyrrhotite and gold Type 1. Pyrrhotite occurs as large patches, or stock-work between silicates (mostly quartz), infrequently in parallel bands.

Stage 2:

Stage 2 is characterised by the absence of pyrite with the dominant sulphide being arsenopyrite Type 2. The arsenopyrite is found as separate euhedral crystals disseminated in the silicates (quartz-carbonate veins).

Stage 3:

Gold Type 2 (Fig. 18a,b) at the New Consort mine occurs as large free gold grains (>100 μm), hosted in the silicates (mainly quartz). Backscatter electron images show that some gold Type 2 grains in this mine have poikilitic micro-textures, with euhedral negative crystals (3-4 μm) (Figs 19, 20), suggesting possible pre-existence of a euhedral phase inside the gold grains. This gold type fills the spaces between grains in the saccharoidal quartz reefs, and displays a variety of morphologies, such as subhedral shapes, long laths, and aggregates.

3. 3 Correlation between the three mines

Based on the textural characteristics and ore mineral associations, two distinctly different types of gold and associated sulphides were distinguished at the three different mines. , occurring in three different stages. Stages 1 and 2 are the sulphide assemblages, and Stage 3 contains the gold Type 2 in quartz veins. The correlations between the three mines are given in Tables 2 and 3. Based on the textural associations, the mineralisation in the different stages occurred sequentially: the sulphide mineralisation of Stage 1 was followed by Stage 2, and after that the silicate vein hosted mineralisation of Stage 3.

3.4 Mineral chemistry

Texturally, two distinct generations each of arsenopyrite, pyrite, and gold have been identified. The morphology and associated minerals which give rise to this classification are shown in Table 1. These two different textures are found in all three of the mines, but one of the textures tends to predominate on the sample scale, with only a few of

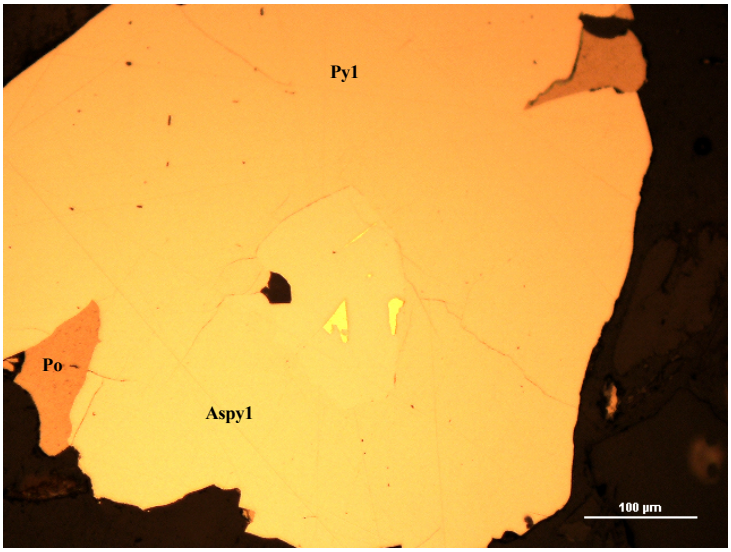

Figure 17: Gold Type 1 (yellow) within sulphides, pyrite Type 1 (Py1), arsenopyrite Type 1 (aspy1), pyrrhotite (Po) from New Consort Mine.

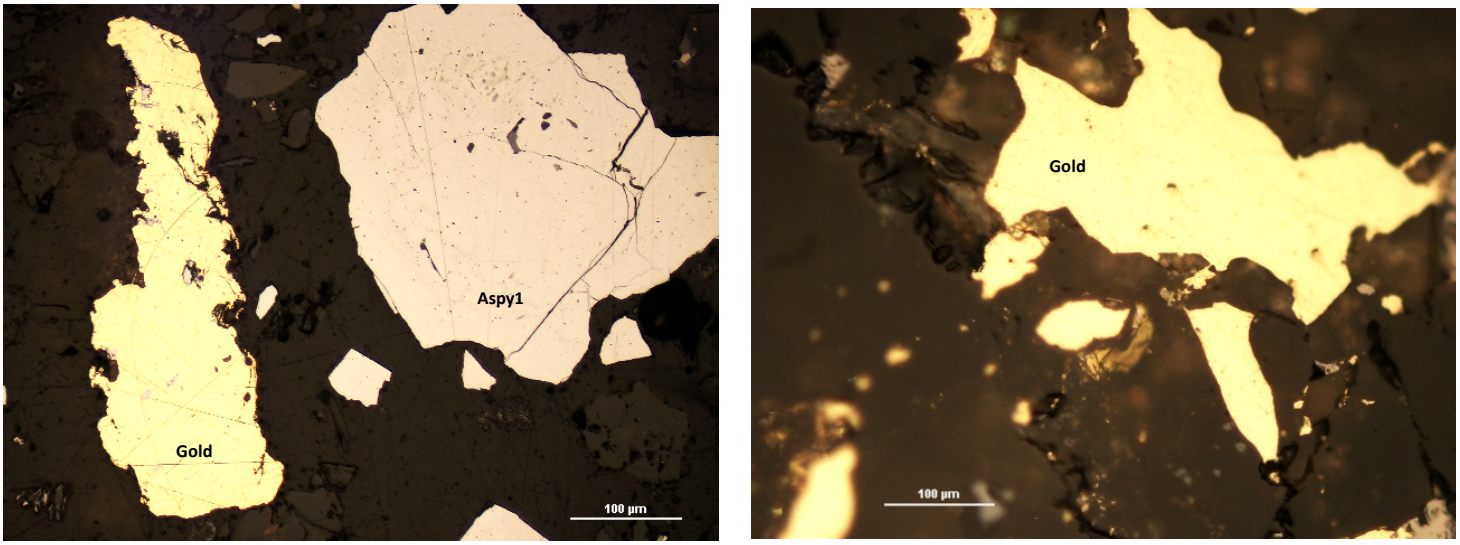

Figure 18: A (left): arsenopyrite Type 1 (Aspy) from New Consort (125906), adjacent to gold Type 2. B (right): Gold Type 2 in silicates from New Consort Mine.

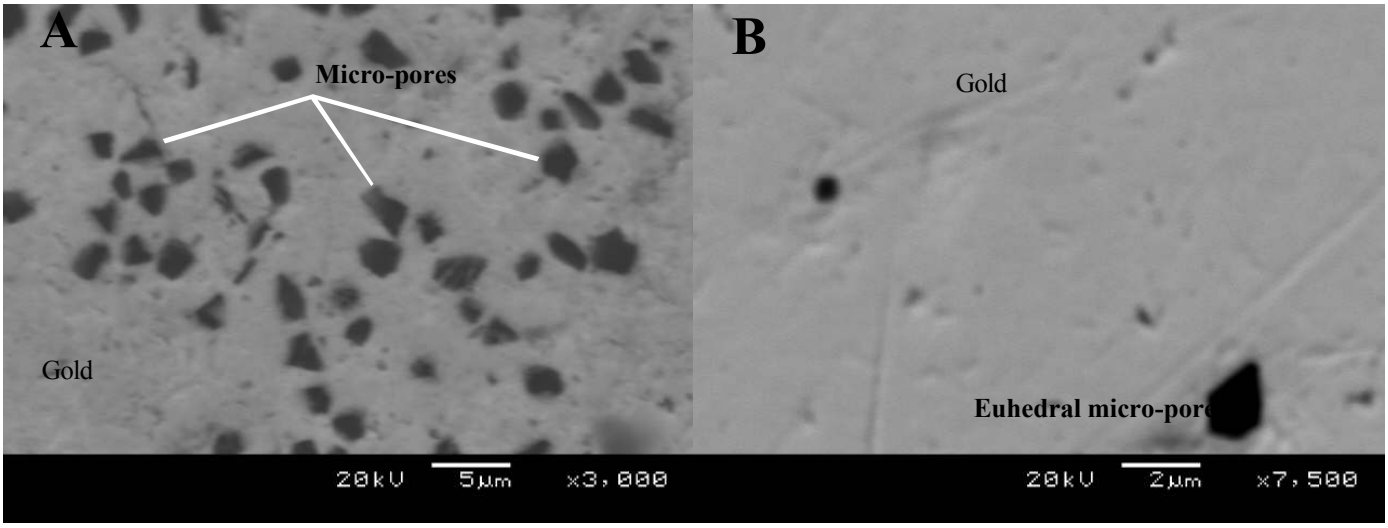

Figure 19: Back-scattered electron images of gold Type 2 grains from the New Consort Mine, illustrating the euhedral negative crystals in the gold grains. These negative crystals represent soluble inclusions (*e.g.* halides) which were lost during sample preparation.

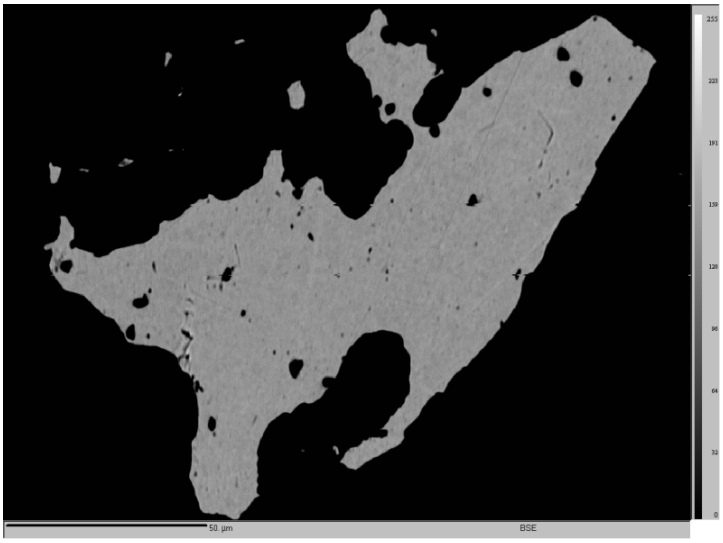

Figure 20: Back-scattered electron image of a gold Type 2 grain from the New Consort Mine, illustrating the euhedral negative crystals in the gold grains.

Table 3: The stages of mineralisation observed at the three mines.

Assemblage	Sheba	New Consort	Fairview
Stage 1: pyrite Type 1, arsenopyrite Type 1, anhedral chalcopyrite, porous pyrrhotite, gold Type 1	Observed	Observed	Observed
Stage 2: pyrite Type 2, arsenopyrite Type 2, euhedral chalcopyrite, massive pyrrhotite, no visible gold	Observed	Arsenopyrite is the only sulphide observed. Pyrite 2, euhedral chalcopyrite, massive pyrrhotite were not observed	Observed
Stage 3: gold Type 2 in silicates	Observed	Observed	Observed

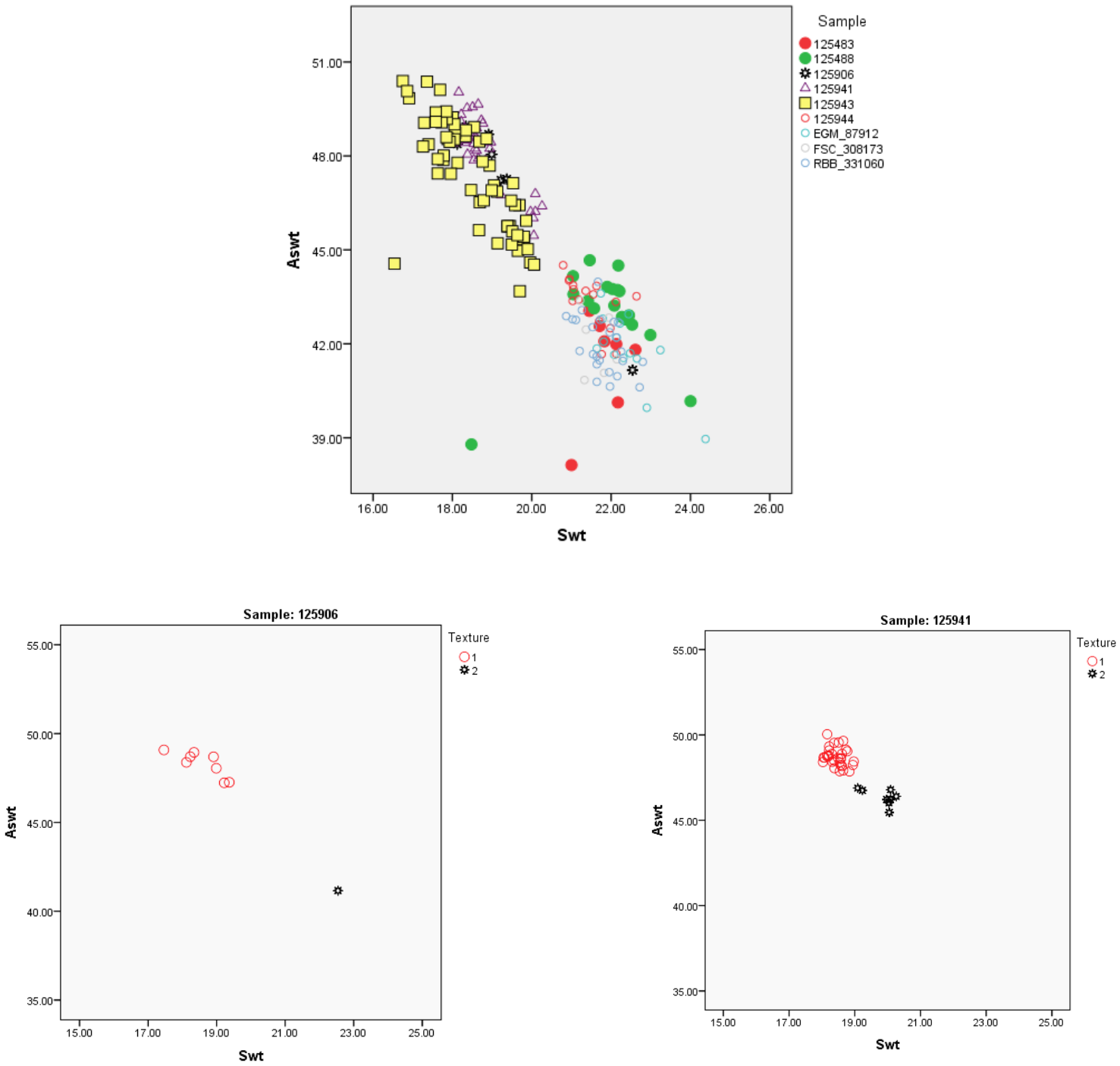

Figure 21: The As content in the initial As-rich arsenopyrite is quite variable, which accounts for the apparent misidentification based on texture, which can be seen in Fig. 20 for samples 125906 (New Consort) and 125941 (Sheba). Typically, only one generation is identified per sample in this study.

samples which display both textural generations. Mineral-chemical support for the textural sub-division into different generations was therefore sought, looking at the results of EPMA and LA-ICP-MS analyses.

Arsenopyrite

The EPMA results show two distinct arsenopyrite groups which correlate with the textural subdivision, although this correlation is not clear-cut, as is shown in Fig. 21. Evolutionary trends within one sample can be seen where the initially formed arsenopyrite Type 1 has higher Ni, Co and As and lower Fe and S than the later generation Type 2 (Fig. 21). Even though the As content in the initial As-rich arsenopyrite is quite variable, which accounts for the apparent occasional misidentification based on texture (which can be seen in Fig. 21 for samples 125906 (New Consort) and 125941 (Sheba)). Typically, only one generation per sample is identified in this study. In terms of minor elements it is noteworthy that the arsenopyrite Type 1 is distinctly enriched in Ni and Co, although these two elements show no significant correlation with each other or the As content of the arsenopyrite. These features are seen in all three mines, confirming the classification based on petrographic observations. The trace element distributions within the arsenopyrite from the three mines, apart from the Ni and Co, do not show a distinct separation between the two types, and are quite variable.

Pyrite

The major sulphide present in the Barberton gold ores, pyrite is texturally subdivided into two main types (Table 2). The first of these, pyrite Type 1, occurs as cores to pyrite grains and may appear porous due to the large number of other mineral inclusions. The second textural type, pyrite Type 2, occurs as rims to pyrite Type 1 cores, and as distinct euhedral grains. It is quite clean in appearance with few inclusions. A clear chemical distinction between the two types is not possible with the EPM results of this study, in contrast to the case with arsenopyrite. The pyrite Type 1 (porous or inclusion-filled cores) correlates with the early poikilitic pyrite (Stage 1 of Agangi *et al.* (2014)), and the pyrite Type 2 correlates with their arsenian pyrite or main pyrite stage (euhedral and rims of Type 1) (Stages 2 and 3 of Agangi *et al.* (2014)).

Pyrite Type 1 of Fairview and Sheba mines have a similar composition. LA-ICP-MS mapping of pyrite from the Sheba mine, however, reveals that the Type 1 pyrite cores are enriched in Sb, Cu, Pb and Au compared to the Type 2 pyrite rims. The LA-ICP-MS mapping confirmed the occurrence of sub-microscopic gold grains in pyrite Type 2. It is also quite distinct that the distribution of Co and Ni occupy different zones within pyrite (Figs 6, 7) and do not correlate with each other. The heterogeneity and zoning features are common in both pyrite types, and are indicative for multi-depositional stages, different timing, and various sources for mineralized fluids (Deditius, *et al.*, 2014).

Pyrite is rarely found among the sulphides of the New Consort mine, which might be due to the relatively high formation temperature (up to higher amphibolite facies) of these ores (Hu *et al.*, 2006) and the decomposition of

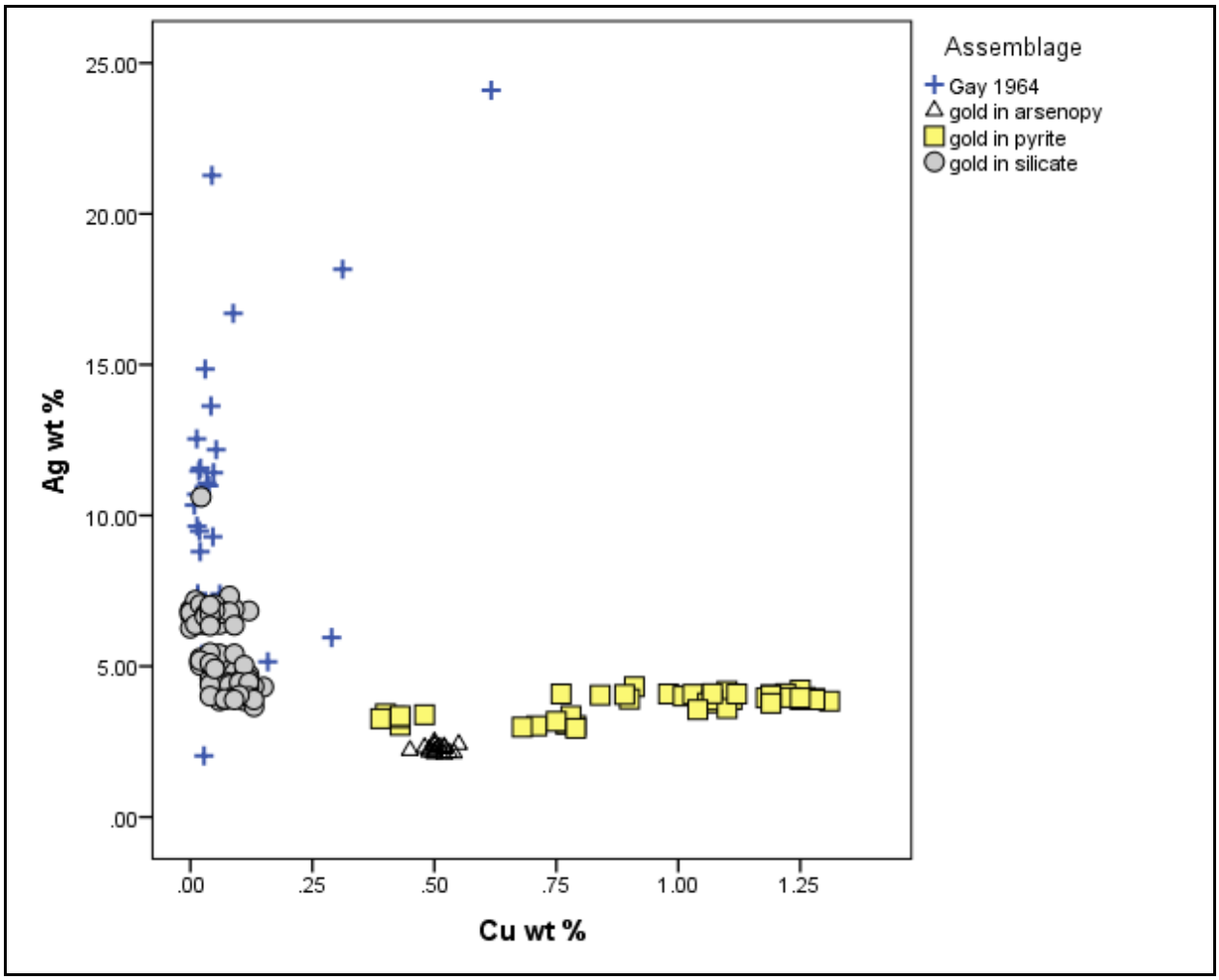

Figure 22: Plot showing the distinct discrimination of gold Type 1 in sulphides, with its higher Cu content, and the gold Type 2 in silicates with its higher Ag content. The blue crosses refer to analyses from Gay (1964) for gold from mines across the BGB, which all appear to belong to the silicate-associated gold.

.

pyrite to pyrrhotite, as well as the oxidation to magnetite or hematite, depending on the prevailing local intrinsic conditions. Pyrite Type 1 has the highest values of Hg among the sulphides in this mine.

Gold

Texturally, gold is found in two distinct assemblages (see Table 2). Gold Type 1 is found as inclusions in sulphides, mainly associated with pyrite Type 1 and arsenopyrite Type 1. Gold Type 2 occurs as much larger grains isolated in silicate assemblages. A clear distinction is possible between the two gold types based on their Ag and Cu contents. The sulphide-associated gold Type 1 grains are enriched in Cu relative to the silicate-associated gold Type 2, which has a higher Ag content (Figure 22).

Semi-quantitative LA-ICP-MS results reveal that arsenopyrite type 1 of the Fairview mine contains the highest content of invisible gold, followed by pyrite Type 1 and anhedral chalcopyrite. However, quantitative EMP results show no systematic relationship between gold and arsenic in pyrite; this was also confirmed by LA-ICP-MS. The LA-ICP-MS analyses indicate that the anhedral chalcopyrite of the Fairview Mine contains chemically bound gold. EMP results show that the gold content in Ni-rich arsenides of the Fairview Mine is higher than in pyrite, arsenopyrite, or pyrrhotite.

Backscatter electron images of gold Type 2 grains from the New Consort mine show euhedral negative crystals (Figs 19, 20), suggesting the presence of soluble phases inside the gold grains which were lost during sample preparation. This would account for the detection of halogens by LA-ICP-MS, when the laser ablates deeper into the grain encountering these inclusions.

Halogens

There are varying amounts of halogens in the sulphides and gold analysed by LA-ICP-MS, from all the stages at the three mines, some with significant amounts of Cl, Br, I, and Na. Gold and pyrite have the highest values of Cl and Na (Fig. 23). Based on the Cl, Br and Na relationships, gold and pyrite (and to lesser degree chalcopyrite, pyrrhotite, and arsenopyrite) in both New Consort and Sheba mines can be divided into two types. The Fairview ores, however, do not show any differences. In New Consort and Sheba Mines, the Cl-Br contents in gold and pyrite show a gap in concentration, whereas in the Fairview Mine Cl and Br show a continuous concentration trend. Br contents in gold are higher than in sulphides. Na and Cl concentrations are variable within the gold and sulphides. Iodine contents in gold and associated sulphides reveal two concentration trends.

There is a positive trend between Hg and the halogens Cl, Br and I in the bulk of the analyses. This is interpreted as being possibly due to sub-microscopic inclusions of Hg-containing halogenides (*e.g.* calomel (HgCl) and kuzminite (Hg(Cl,I) - see Fig. 24). This feature is found in both textural assemblages and in all minerals. The presence of euhedral negative crystals in gold Type 2 grains from the New Consort mine (Figs 19 & 20) indicate the presence of water-soluble phases, most probably halides (*e.g.* halite (NaCl) and sylvite (KCl)).

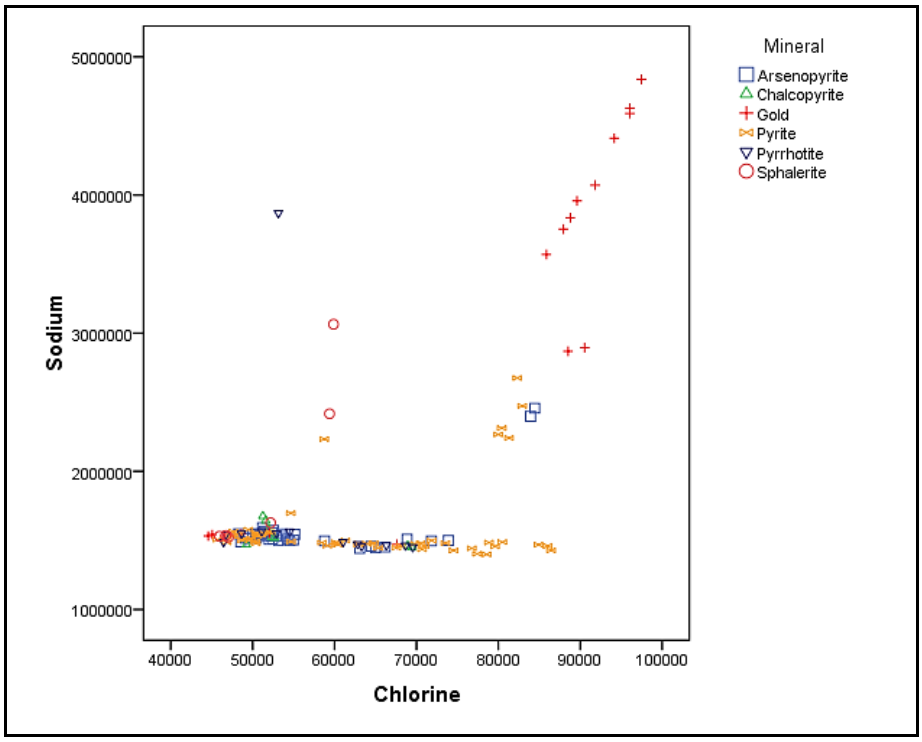

Figure 23: A plot of Na vs Cl, showing the positive correlation of the two in some of the gold, as well as some pyrites and arsenopyrite. This correlation is consistent with the presence of NaCl inclusions in the gold, as pictured in Figs 16 & 17 above.

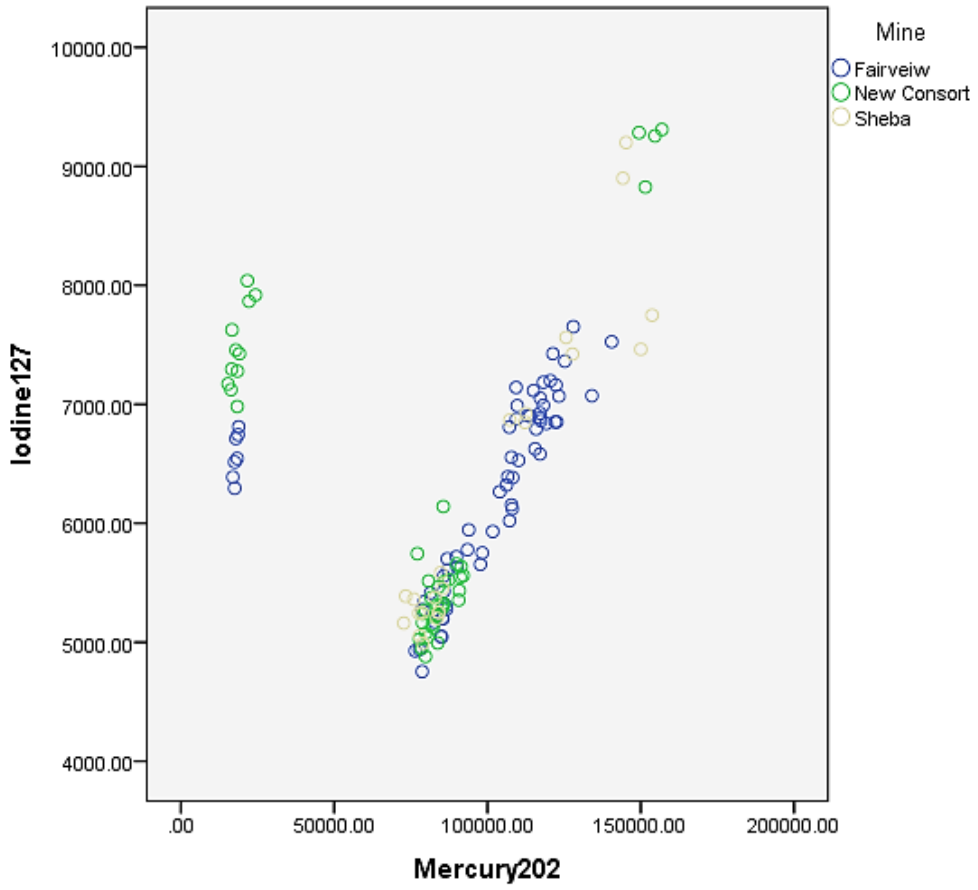

Figure 24: Plot of counts (cps) obtained by LA-ICP-MS for the range of minerals, from both Type 1 and Type 2, from the three mines. There are two distinct Iodine bearing trends, one without Hg, which could relate to the type of phase occurring as inclusions. This behaviour is similar for Cl and Br.

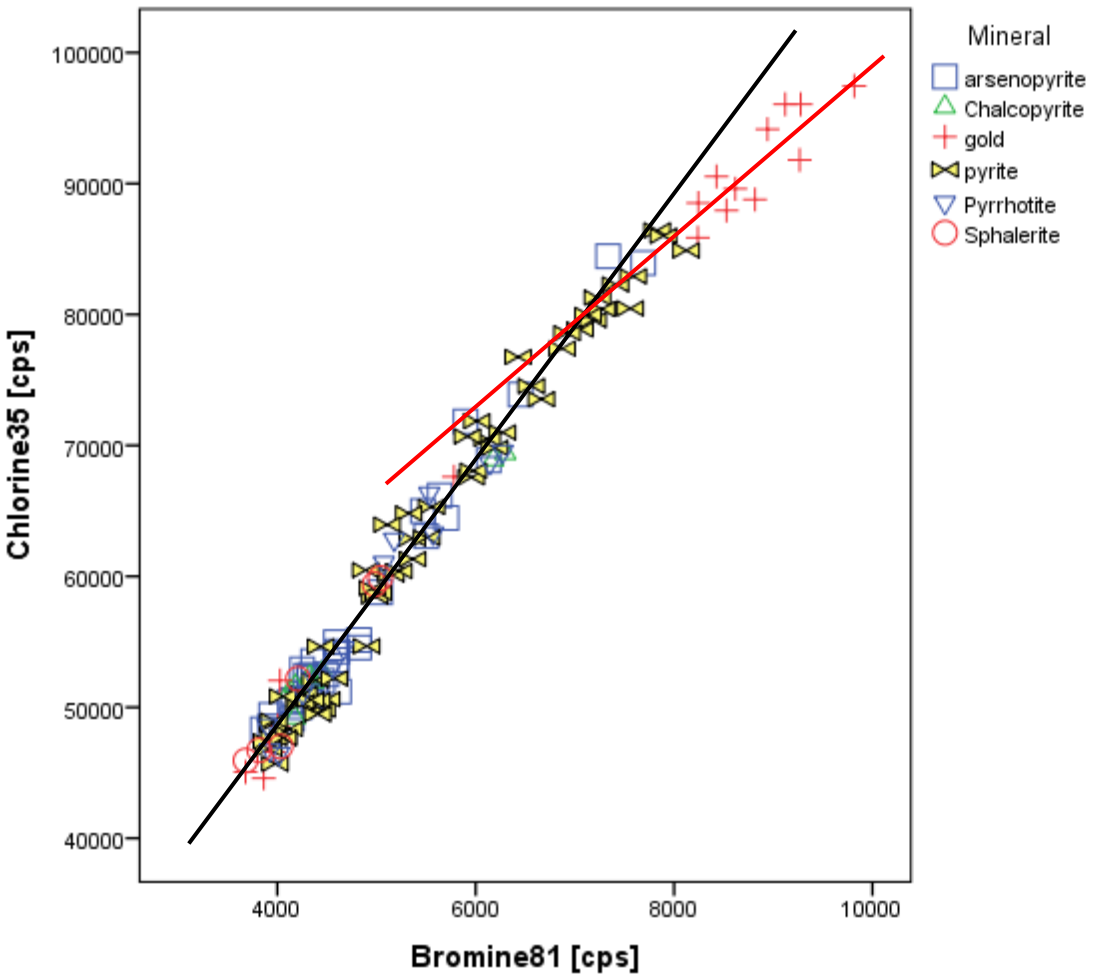

Figure 25: Plot of Cl vs Br cps for all mineral phases (of both Types) at all mines. Gold Type 2 and a few sulphides (along the red trend line) were deposited in an environment with a higher halogen content and a different $^{35}Cl/^{81}Br$ ratio to the gold Type 1 and the bulk of the sulphides (along the black trend line).

The LA-ICP-MS halogen data show that there are two trends in Cl/Br ratios (Fig. 25), and within them are characteristic associations (clusters), which are independent of a specific mineral, sample, or mine. This clustering is clearly seen in the plot of Cluster 2 (pyrite Types 1 and 2 from New Consort, and pyrite Type 2 from Sheba) and Cluster 1 (gold Type 2 from New Consort, and arsenopyrite Type 1 from Fairview). Clusters 1 and 2 appear to be related (they have similar slopes), despite the prominent difference in mercury, and are not related to Cluster 0 (the balance of the analysed minerals). This implies the following:

- Similar precipitation conditions (or mechanisms) from intrinsically different fluids for Cluster 0 and 2 and
- Distinctive differences in the precipitation mechanism of Cluster 1.
- The pyrite Types 1 and 2, as distinguished texturally, do not exclude formation from the same type of fluid (differences possibly due to early and late formation within one event).
- The same textural Type can precipitate from different fluids, implying that the precipitation mechanism (not the fluid type) is responsible for differences in textures.

4. Discussion

The mineral assemblages and remnant primary bedding structures in the rocks of the Fairview and Sheba mines indicate low-grade, greenschist facies metamorphism (Miyashiro, 1973; Stiegler *et al*., 2010), while rocks of the New Consort mine reflect medium- to high amphibolite facies (indicated by hornblende) (Dziggel *et al*., 2007; 2010.)

4.1 Fairview mine lithology

In sample FSC-308168, the presence of a relatively high-grade assemblage (biotite, actinolite, plagioclase, and hornblende) is indicative of the presence of basic volcanics in the source rocks of the Fairview Mine (De Vries *et al.,* 2006; Hessler & Lowe, 2006). The presence of muscovite in the arenites of the Fairview Mine indicates the pre-existence of argillaceous layers within the source of these rocks (Dziggel *et al*., 2002; De Vries *et al*., 2006; Hessler & Lowe, 2006). Two foliation directions are distinguished in most of the Fairview mine lithology, which indicate interfolial folds associated with shearing, or may have formed due to primary cross-bedding structures that are associated with alluvial and braided-fluvial sandstones of the Moodies Group (Eriksson *et al*., 2001; Hessler & Lowe, 2006).

Brecciation is a common feature in the Fairview arenites, which indicates shearing and faulting episodes. Angular fragments imply short transport distance from the sources. The resultant fracture porosity represent the most favourable structures to host gold mineralization in this area (Groves *et al*., 1998; McCaffrey *et al*., 1999). Compositional immaturity, and the presence of feldspars probably suggests un-noticeable weathering of the source terrain or short transport distances (Hofmann, 2005).

The extensive quartz-carbonate veining suggests later hydrothermal activity (De Vries *et al*., 2006). Silicification and carbonation processes are very distinctive in the rocks and associated ores of the Fairview Mine. These processes are associated with a depletion of some elements during interactions between seawater and ancient Fairview rocks (source of gold), such as Ni and Co and some other mobile metals (Cu, Zn). However, K, Rb, and

Ba were later enriched in these rocks due to the metasomatism that resulting from granitic intrusions. Large and euhedral quartz indicates an imprint of thermal metamorphism on these rocks.

4.2 Sheba mine lithology

Most of the samples examined are dominated by quartz, calcite, biotite, muscovite, garnet and chlorite. This mineral assemblage indicates that the Sheba Mine rocks formed under low greenschist metamorphic facies (Stiegler *et al.*, 2010; Miyashiro, 1973). Locally, high amphibolite facies (indicated by hornblende from the lithology of nearby New Consort and Fairview mines) may be due to late granitic intrusions. Generally, the rocks of the Sheba Mine can be subdivided into quartz-rich arkoses, metapsammite, and metapelites. Hessler & Lowe (2006) suggested that the basal conglomerates of the Moodies Group (present at the Sheba Mine) were derived from volcanic and sedimentary rocks of the Swaziland Supergroup. They indicated that felsic volcanic rocks, cherts, silicified ultramafic fragments, and quartz veins dominate the sedimentary clasts of the Moodies Group.

The dissolution and re-crystallization of the quartz during prograde metamorphism formed a new generation of small (120^0 triple-junction) quartz polygons. This texture indicates textural equilibrium during the re-crystallization at higher temperatures coupled with a lack of deformation (Barrie *et al*., 2010). The quartz contents in the Sheba greywackes indicate a major granitic component (McLennan, 1984), and stringers of graphite characterize the arkoses and metapelites, reflecting an early existence of organic materials across these sediments.

Quartz and carbonate veins are common in the majority of the Sheba Mine's rocks. Most of these veins were deposited concordantly with either relicts of primary bedding, or the foliation planes, while some of these veins filled the shearing planes. The shape, symmetry, and the interaction of these veins with the country rocks suggest late injection. These quartz-rich veins may form due to a recent magmatic hydrothermal activity (De Vries & Touret, 2007) or due to dehydration that was caused by prograde metamorphism

The mineralogical relationships in the Sheba rocks indicate multiple metamorphic episodes affecting the lithologies of the BGB. The first was regional, which affected the mafic and ultrabasic rocks, and is associated with early tectonism, producing greenschist metamorphic facies. The second episode is a prograde thermal and/or regional type that produced a higher-grade metamorphic facies (high greenschist, low amphibolite facies), which is found in the vicinity of granitic intrusions. The third event is dynamic metamorphism associated with shearing, which caused brecciation and fracturing . This resulted in structural porosity for the syn-to late genetic mineralized fluids (Dirks *et al*., 2013). All these metamorphic episodes resulted in changes to the mineralogy and morphology of the rocks of the Sheba Mine.

4.3 Mineralising events

The main host rocks of gold mineralization in these mines belong to the Fig Tree and the Moodies Group sedimentary rocks (Dziggel *et al.*, 2007). However, gold is found in variable amounts in all of the BGB rock types (Dirks *et al.*, 2013), which is indicative of pervasive fluid flow and extensive fluid–wall rock interaction over long periods of time (Bierlein & Maher, 2001). The majority of the gold is associated with quartz-carbonate veins (Stage

3) with mineralized fractures spatially proximal to large-scale compressional and/or shear zones (structural porosity) (Dziggel *et al.*, 2007, 2010; Dirks *et al.*, 2013). Most of the gold deposits are located in the second and third order structures (Dirks *et al.*, 2013), or in the fault intersections, corresponding to places of low stress, which increases fluid passage. The structural patterns of gold mineralization in the studied mines are similar to that of Pilbara in Western Australia (Thèbaud *et al.*, 2008).

The mineralization in these mines postdates the peak of metamorphism. Auriferous mineralising fluids are usually characterized by P-T conditions of ca. 200–650° C and 1–5 kbar, low salinity, and high CO_2. These fluids are generated from metamorphic devolatilisation, and metamorphic reactions in the middle and lower crust (Dziggel *et al.*, 2007; Pettke *et al.*, 1998), or are alternatively of magmatic origin (Hoffman, 2005; Vanko, 1986).

The dominant sulphides of these mines are pyrite, arsenopyrite, and pyrrhotite, with minor Ni-rich arsenides. This assemblage is similar to that of the mesothermal gold ores in the Archaean Yilgarn Craton of Western Australia (Vaughan & Kyin, 2004). Both of these types of gold deposits are characterized by late-stage low-sulfide quartz veins, that occur at trans-crustal strike-slip and thrust faults, which are associated with collision. The faults provide conduits for the large volume of fluids, which were generated during the collision and the associated metamorphic dehydration. This fluid flows into upper levels of the crust where the gold deposits are formed (Groves *et al*., 1998). The gold of the studied mines occurs in two distinct assemblages, representing two different mineralization stages. The late Stage 3 gold may have been derived due to remobilization of gold in the earlier stages, or due to different fluid sources.

Gold mineralization at the New Consort Mine formed at relatively higher temperatures (Dziggel *et al.*, 2007) compared with the Sheba and Fairview mines (De Ronde *et al*., 1992; Agangi *et al*., 2014). This has been alternatively attributed to different ore-forming processes (Dziggel *et al.*, 2007) or a zonation outwards from the epicentres of the mineralising fluids at Agnes and New Consort and Sheba (Gribnitz, 1961; Gay, 1964), which correlates well with the structural controls described by Dirks *et al*. (2013).

Tomkinson & Lombard (1990) suggested a formation temperature of gold in pyrite and arsenopyrite above 500^0C, which results in gold that appears to be of primary origin, as indicated by the gold grain morphology. The gold grains, therefore, appear to change their texture rather than chemistry during metamorphism. Nevertheless, EMPA and LA-ICP-MS results revealed at least two chemically different gold types in the studied mines. The EMPA results show that the compositions of arsenopyrite Type 1 are very similar in all mines, and similarly for Type 2, reflecting a common origin for the mineralising fluid over the area, in which the physical parameters (temperature, pressure) were similar but the dissolved trace elements in the fluid, which are reflected in the trace element compositions of the various minerals, owe their variation to the local source from which they were scavenged by the fluid.

The sources of the fluids, which precipitated ores in the study area, are uncertain. However, dehydration of meta-volcano-sedimentary rocks in greenstone belts has been recognized as a significant source of fluid during regional

metamorphism, causing intense metasomatism and ore deposition (Saha & Venkatesh, 2002; Dziggel *et al.*, 2007; Ordonez-Calderon *et al.*, 2008).

4.4 Halides

We observe systematically different counts for chlorine during laser ablation of ore minerals (including gold) in different populations (i.e. different types, stages, assemblages) of ore minerals. The relatively small overall scatter of $^{37}Cl/^{35}Cl$ ratios for all analyses (Spearman's rho = 0.969 for 197 analyses), and the presence of the same types of minerals in both populations (high and low Cl) implies that the ablated mineral species is not responsible for the observed differences in Cl counts. Argon was used as a carrier gas and it stands to reason that the elevated counts for ^{37}Cl can be attributed to $^{36}ArH^{+}$ (Fietzke *et al*. 2008), although in our analyses, this was not quantified. Taking this into consideration, the consistent results obtained point to small, but significant, differences in $^{37}Cl/^{35}Cl$, Cl/Br, and Cl/I ratios between the populations. Small gold grains in the sulphide-rich assemblages are low in chlorine, compared to the coarse gold (rarely associated with sulphides) in the silicate matrix.

The complexing of gold and its precipitation to form ore deposits has been extensively reviewed (e.g. Mikucki, 1998; Groves *et al*., 2003; Goldfarb *et al*., 2005; Simmons *et al*., 2005; Phillips & Powell, 2009). It is obvious that ore-forming fluids in metamorphic terrains are typically low-salinity fluids (*e.g*., Groves, 1993; Hammond *et al*., 2007), with thio-complexes the most likely transport mechanisms for gold. By interaction with iron-containing rocks under suitable intrinsic conditions, small amounts of gold will be precipitated as a consequence of loss of the complexing sulphur to form base metal sulphides. The gold Type 1 (characterized by low Ag, low Cl, and high Cu counts) arguably formed through this process.

It has been argued frequently that dramatic pressure fluctuations as a consequence of seismic activity (Sibson *et al*., 1975; Sibson, 1987; Micklethwaite & Cox, 2004) may lead to phase separation (*i.e*. boiling of the hydrothermal fluid) and a consequent deposition of coarse gold (Groves & Foster, 1991). Boiling of hydrothermal fluids (Haas, 1971; Bischoff, 1980; Bischoff & Pitzer, 1985) without a pressure drop is not considered likely because of the prevailing lithostatic pressure. Loucks & Mavrogenes (1999) argued that complexing sulphur could be lost from the gold complexes due to the pressure change alone, leading to gold precipitation. Simmons *et al*. (2005) argue that boiling efficiently removes gold and silver from the fluid and leads to precipitation, as is exemplified by fluid compositions after precipitation of gold in geothermal production wells in New Zealand (Brown, 1986). Elevated Ag-contents in native gold have been associated with boiling at moderate to high temperatures and high chlorine contents of the fluid (Cole & Drummond, 1986). However, the elevated chlorine concentrations in our gold Type 2 and some sulphides require not only a mechanism to increase manifold the chlorine concentration from the typically low fluid levels (*e.g*. Liebscher, 2010), but also a mechanism of preservation within the ore minerals.

There is no compelling geological evidence (besides our tentative suggestion that differences in chlorine isotopes and halogen ratios may exist) that would suggest a relatively late fluid of distinctly different origin, that could be called upon to explain a much higher salinity. An increase in salinity by extensive boiling appears to be the most

acceptable option. The textural occurrence of our gold Type 2 is consistent with a scenario of precipitation during boiling.

Chlorine contents in native gold (or electrum) are rarely looked for or reported. If reported, it is logically assumed that the chlorine (similar to a range of other elements such as He, U, or Th) is not incorporated into the mineral lattice but rather represents (fluid) inclusions (Zaikin & Moiseyenko, 1987; Semenko, 1990; van Hees *et al*., 1992; Eugster, 1995; Pettke *et al*., 1997). Because of the sparsity of halogen data, it is close to impossible to evaluate how common elevated chlorine contents in native gold are, and what the significance of our observation in relation to the ore-forming processes of other gold mineralizations may be. For example, Moisyenko & Mironyuk (1998) report not only highly variable chlorine and salt concentrations in native gold within and between deposits, but also a systematically higher level compared to coexisting (?) quartz. They vaguely attribute the difference in salinity to a "border effect" and the hydrophobic character of gold. Boer *et al*. (1995) describe fluid inclusions in quartz and in native gold, but only report HCl concentrations for the inclusions in quartz.

We were not able to find any studies that would allow us to evaluate whether the shape of fluid inclusions in native gold may be diagnostic. The pictures in Boer *et al.* (1995) may be interpreted that round or irregular shapes are to be expected. However, in polished sections, the almost inevitable smearing of metals during polishing (Franklyn & Merkle, 2001; Makovicky *et al*., 1990) may disguise the true shape of inclusions, especially if they are very small. In contrast to the intuitive expectation that fluid inclusions should be rounded or irregular, we observed inclusions in gold Type 2 grains which are without doubt euhedral. We have at present no way to evaluate convincingly whether these shapes represent a negative crystal form of the host gold, or whether they represent euhedral inclusions which were dissolved and washed away during the polishing process. The ablation of the minerals volatilized inclusions below the surface and led to the observation of high halogen counts, but this does not allow the determination of their nature. Considering the precipitation of gold from a fluid, and the very low probability of gold to form euhedral habits, we feel that gold is very unlikely to form negative crystal forms around fluid inclusions. We prefer the interpretation that these textures represent minerals co-precipitated with the gold and that these mineral inclusions are, as implied by the high chlorine counts and their solubility, rich in chlorine and probably chloride. This is unusual, considering that salinity in fluid inclusions of lode gold deposits are typically considered to be low (*e.g.* Wilkinson, 2001) and boiling to the degree of halide precipitation appears very uncommon.

However, halite and sylvite have been observed, not only in a skarn environment (*e.g.*, Fulignati *et al*., 2001), but also in metamorphic rocks of amphibolite to granulite facies as solid inclusions (Trommsdorff *et al*., 1985; Markl & Bucher, 1998), where they may be attributed to boiling (Erwood *et al*., 1979; Cloke & Kesler, 1979; Trommsdorff & Skippen, 1986; Campbell *et al*., 2001) or extensive desiccation of migrating fluids. Our samples with Cl-enriched gold are of amphibolite facies, which is tentatively attributed to the thermal effect of granitic intrusions nearby. Boiling would be a plausible mechanism for precipitation of coarse-grained gold in our samples, but a slow desiccation process not.

Even in hydrothermal mineralization, halite has been observed. Campbell *et al*. (2001) describe halite inclusions in vein quartz and discuss in detail the evolution and fluid compositional evidence for the "halite trend", *i.e*. the evolution of fluid compositions as a consequence of halite crystallization. Although the "halite trend" is implied by several fluid inclusion studies (*e.g*. Cloke & Kesler, 1979; Campbell *et al*., 1995), mineralogical evidence in the form of halite inclusions in rock forming minerals is typically absent. It is noteworthy that crystallization of halite will increase the Br/Cl ratio of the fluid. Our gold Type 2 defines a trend of a higher Br/Cl ratio (in counts per second) than the ore minerals with lower chlorine content. The "halite trend" also implies that the crystallizing halite will be K-containing (Campbell *et al*., 1995, 2001). The analyses of our gold Type 2 imply a positive correlation between Na and K (Spearman's rho = 0.827 with a two-sided error probability of 0.002 for 11 analyses). In the low chlorine minerals, no systematic relationship between Na and K is detectable.

Yermolayev *et al*. (1993) present to our knowledge the only study related to gold mineralization, which may lend some support to our opinion, that the negative forms in the native gold Type 2 may be solid halides. They found that quartz in their study material contained euhedral crystals of halite and sylvite whenever there is gold in the samples. They write "It is important to note that these are not daughter minerals from the inclusions, but solid crystals in the silica mass". The association of halides with adularia in this deposit may be considered a strong indication of boiling as the process of gold deposition.

Heinrich *et al*. (2004) and Heinrich (2005) evaluated the transport and deposition of gold across a large temperature and pressure range. Their modeling implies that fluid-vapour separation (and the generation of a hypersaline fluid) is possible over a wide range of conditions. If the fluid coexists with muscovite and feldspar (as is the case in our samples), gold solubility in the fluid drops dramatically, even at high temperature.

Although HCl may be lost during vapour formation, sodium, gold, silver, and copper are concentrated in the fluid in sulphur-free systems. However, gold may participate into the vapour phase if sufficient concentrations of sulphur are available (Pokrovski *et al*., 2013). Compositions of hypersaline fluid inclusions (Kouzmanov & Pokrovski, 2012; Pokrovski *et al*., 2013) imply a strong tendency for gold to partition into the vapour phase. Weatherley & Henley (2013) found that cavity expansion during an earthquake generated such extreme reductions in pressure that fluids expand to a low-density vapour, resulting in the rapid co-deposition of silica together with a variety of trace elements to form gold-enriched quartz veins. This process continues until the pressure has recovered to ambient conditions. The textural relationships between our gold Type 2 and rare sulphides is consistent with fluids with a low concentration of sulphur.

It appears that with present knowledge from natural examples and experimental investigations, different precipitation mechanisms for the ore minerals are indicated. Compositional and textural variations in pyrite and arsenopyrite and gold Type 1 textures, as well as minor element associations and concentrations imply that the bulk of the ore minerals were precipitated from a range of hydrothermal fluids typical for greenstone gold mineralization. Fluid compositions and intrinsic parameters varied, as must be expected for a terrain of such complex geological history as the Barberton Greenstone Belt. However, gold Type 2 (of Stage 3) implies a

different fluid composition that was saturated in NaCl and followed the “halite trend”. Boiling was in all likelihood responsible for the deposition of gold and the co-precipitation of a halide, probably halite with a narrow range of Na/K ratios.

5. Conclusions

The gold mineralisation in the Barberton Greenstone Belt was the result of a pervasive hydrothermal event that post-dated main tectonic and metamorphic events. This hydrothermal event was strongest at the conjunction of structural features in the New Consort/Sheba/Fairview and Agnes areas. The mineralisation took place over a long period, and most probably consisted of many individual pulses, at varying depths, giving rise to the variation in the ore mineral parageneses and chemistries described above.

The identification of the high concentrations of halogens and their isotopic ratios in sulphide minerals and native gold affords the possibility to add a new facet to the study of mineralizing processes. Appropriate analytical protocols are needed to evaluate the potential of this aspect, especially a sample preparation protocol which will allow the preservation and recognition of solid, but water soluble inclusions in opaque minerals.

Although impossible to quantify at this point in time, our findings imply a more intricate mineralization history in the Barberton Greenstone Belt than meets the glancing eye.

Acknowledgements
We thank the late Peter Gräser (EPMA; University of Pretoria) and Herman Espach and Eduan Naude (LA-ICP-MS; Forensic Science Laboratory) for assistance with analyses. Support for the first author was provided by Alneelain University.

6. References

Agangi, A., Hofmann, A. and Przybyłowicz, W., (2014). Trace element zoning of sulfides and quartz at Sheba and Fairview gold mines: Clues to Mesoarchean mineralization in the Barberton Greenstone Belt, South Africa. Ore Geology Reviews, 56: 94-114.

Anhaeusser, CR. 1976. The nature and distribution of Archaean gold mineralization in southern Africa. *Mineral Science Engineering*, **8**, pp. 46-84.

Anhaeusser, CR. 1986. Archaean gold mineralization in the Barberton Mountain Land. In: Anhaeusser, CR., Maske, S. (Eds.), Mineral Deposits of Southern Africa. *Geological Society of South Africa*, Special Publications, pp. 113–154.

Barrie, CD, Boyle, A, Cook, NJ, and Prior, DJ. 2010. Pyrite deformation textures in the massive sulfide ore deposits of the Norwegian Caledonides. *Tectonophysics*. **483**, pp. 269–286.

Bierlein, FP & Maher, S. 2001. Orogenic disseminated gold in Phanerozoic fold belts—examples from Victoria, Australia and elsewhere. *Ore Geology Reviews*, 18(1), 113-148.

Bischoff, JL. 1980. Geothermal system at 21 N, East Pacific Rise: Physical limits on geothermal fluid and role of adiabatic expansion. *Science*, **207(4438)**, pp. 1465-1469.

Bischoff, JL and Pitzer, KS. 1985. Phase relations and adiabats in boiling seafloor geothermal systems. *Earth and Planetary Science Letters*, **75(4)**, pp. 327-338.

Boer, RH, Meyer, FM, Robb, LJ, Graney, JR, Vennemann, TW, and Kesler, SE. 1995. Mesothermal type mineralization in the Sabie Pilgrim's Rest gold field, South Africa. *Economic Geology*, **90(4)**, pp. 860-876.

Brandl, G, Cloete, M, and Anhaeusser, CR 2006. Archaean greenstone belts. *In*: Johnson, MR, Anhaeusser, CR and Thomas, RJ (Eds.) (2006). *Geology of South Africa*, Geological Society of South Africa, Johannesburg/ Council for Geosciences, Pretoria, pp. 9-56.

Brown, KL. 1986. Gold deposition from geothermal discharges in New Zealand. *Economic Geology*, **81(4)**, pp. 979-983.

Cabri, LJ, Chryssoulis, SL, de Villiers, JPR, Laflamme, JHG, Buseck, PR. 1989. The nature of “invisible” gold in arsenopyrite. *Can. Mineral*. **27**, pp. 353–362

Campbell, AR, Banks, DA, Phillips, RS and Yardley, BW. 1995. Geochemistry of Th-U-REE mineralizing magmatic fluids, Capitan Mountains, New Mexico. *Economic Geology*, **90(5)**, pp. 1271-1287.

Campbell, AR, Lundberg, SA and Dunbar, NW. 2001. Solid inclusions of halite in quartz: evidence for the halite trend. *Chemical Geology*, **173(1)**, pp. 179-191.

Cloke, PL and Kesler, SE. 1979. The halite trend in hydrothermal solutions. *Economic Geology*, **74(8)**, pp. 1823-1831.

Cole, DR and Drummond, SE. 1986. The effect of transport and boiling on Ag/Au ratios in hydrothermal solutions: a preliminary assessment and possible implications for the formation of epithermal precious-metal ore deposits. *Journal of Geochemical Exploration*, **25(1),** pp. 45-79.

De Ronde, CEJ, Spooner, ETC, De Wit, MJ, Bray, CJ. 1992. Shear zone-related, Au quartz vein deposits in the Barberton greenstone belt, South Africa; field and petrographic characteristics, fluid properties, and light stable isotope geochemistry. *Economic Geology*, **87**, pp. 366–402.

De Villiers, JE. 1957. *The mineralogy of the Barberton gold deposits*. Geological Survey of South Africa, Bulletin **24**.

De Vries, ST, and Touret, JLR. 2007. Early Archaean hydrothermal fluids; a study of inclusions from the ~3.4 Ga Buck Ridge Chert, Barberton Greenstone belt, South Africa. *Chemical Geology*, **237**, pp. 289-302.

De Vries, ST, Nijman W, and Armstrong RA. 2006. Growth-fault structure and stratigraphic architecture of the Buck Ridge volcano-sedimentary complex, upper Hooggenoeg Formation, Barberton Greenstone Belt, South Africa, *Precambrian Research*, **149**, pp. 77–98.

De Wit, MJ, Furnes, H., and Robins, B., 2011. Geology and tectonostratigraphy of the Onverwacht Suite, Barberton Greenstone Belt, South Africa. *Precambrian Research*, 186, 1-27 doi:10.1016/j.precamres.2010.12.007.

Deditius, AP, Reich, M, Kesler, SE, Utsunomiya, S, Chryssoulis, SL, Walshe, J, and Ewing, RC. 2014. The coupled geochemistry of Au and As in pyrite from hydrothermal ore deposits: *Geochimica Et Cosmochimica Acta*, **140**, pp. 644-670.

Dirks, PHGM, Charlesworth, EG and Munyai, MR. 2009. Cratonic extension and Archaean gold mineralisation in the Sheba-Fairview mine, Barberton Greenstone Belt, South Africa. *South African Journal of Geology*, **112(3-4)**, pp. 291-316.

Dirks, PHGM, Charlesworth, EG, Munyai, MR, and Wormald, R. 2013. Stress analysis, post-orogenic extension and 3.01 Ga gold mineralisation in the Barberton Greenstone Belt, South Africa. *Precambrian Research*, **226**, pp. 157– 184.

Dziggel, A, Knipfer, S, Kisters, AF and Meyer, FM. 2006. P–T and structural evolution during exhumation of high-T, medium-P basement rocks in the Barberton Mountain Land, South Africa. *Journal of Metamorphic Geology*, **24(7)**, pp. 535-551.

Dziggel, A, Otto, A, Kisters, AFM, Meyer, FM. 2007. Tectono-metamorphic controls on Archaean gold mineralization in the Barberton greenstone belt, South Africa: an example from the New Consort gold mine. In: Van Kranendonk, M., Smithies, R.H., Bennett, V. (Eds.), *Earth's Oldest Rocks. Developments in Precambrian Geology*, vol. **15**, pp. 699–727.

Dziggel, A, Poujol M, Otto A, Kisters, AFM, Trieloff, M, Schwarzd, WH, Meyer, FM 2010. New U–Pb and $^{40}Ar/^{39}Ar$ ages from the northern margin of the Barberton greenstone belt, South Africa: Implications for the formation of Mesoarchaean gold deposits. *Precambrian Research*, **179**, pp. 206–220.

Dziggel, A, Stevens, G, Poujol, M, Anhaeusser, CR and Armstrong, RA. 2002. Metamorphism of the granite–greenstone terrane south of the Barberton greenstone belt, South Africa: an insight into the tectono-thermal evolution of the 'lower' portions of the Onverwacht Group. *Precambrian Research*, **114**, pp. 221–247.

Economou-Eliopoulos, M, Eliopoulos, DG and Chryssoulis, S. 2007. A comparison of high-Au massive sulfide ores hosted in ophiolite complexes of the Balkan Peninsula with modern analogues: Genetic significance. *Ore Geology Reviews*, **33**, pp. 81–100.

Elliot, AD and Watling, HR. 2011. Chalcopyrite formation through the metathesis of pyrrohite with aqueous copper. *Geochimica et Cosmochimica Acta*, **72**, pp. 2103–2118.

Eriksson, PG, Martins-Neto, MA, Nelson, DR, Aspler, LB, Chiarenzelli, JR, Catuneanu, O, Sarkar, S, Altermann, W, Rautenbach, W. 2001. An introduction to Precambrian basins: their characteristics and genesis. *Sedimentary Geology*, (**141-142**), pp. 1-35.

Erwood, R J, Kesler, SE and Cloke, PL. 1979. Compositionally distinct, saline hydrothermal solutions, Naica mine, Chihuahua, Mexico. *Economic Geology*, **74(1)**, pp. 95-108.

Eugster, O, Niedermann, S, Thalmann, C, Frei, R, Kramers, J, Krähenbühl, U, Liu,YZ, Hofmann, B, Boer, RH, Reimold, WU, and Bruno, L. 1995. Noble gases, K, U, Th, and Pb in native gold. *Journal of Geophysical Research: Solid Earth*, **100(B12)**, pp. 24677-24689.

Fietzke, J, Frische, M, Hansteen, TH and Eisenhauer, A. 2008. A simplified procedure for the determination of stable chlorine isotope ratios (d37Cl) using LA MC ICP MS. *Journal of Analytical Atomic Spectrometry*, **23(5)**, pp. 769-772.

Franklyn, CB and Merkle, RKW. 2001. Surface contamination by smearing during polishing–A PIXE study. *Nuclear Instruments and Methods in Physics Research Section B: Beam Interactions with Materials and Atoms*, **181(1)**, pp. 140-144.

Fulignati, P, Kamenetsky, VS, Marianelli, P, Sbrana, A and Mernagh, TP. 2001. Melt inclusion record of immiscibility between silicate, hydrosaline, and carbonate melts: Applications to skarn genesis at Mount Vesuvius. *Geology*, **29(11)**, pp. 1043-1046.

Gay, NC. 1963. A review of the geochemical characteristics of Gold in ore deposits. *University of the Witwatersrand, Economic Geology Research Unit, Information Circular* **12.**

Gay, NC. 1964. The composition of gold from the Barberton Mountain Land. *University of the Witwatersrand, Economic Geology Research Unit Information Circular* **19**, 53 pages

Goldfarb, RJ, Groves, DI, and Gardoll, S. 2001. Orogenic gold and geologic time: a global synthesis. *Ore Geology Reviews*, **18**, pp. 1–75.

Goldfarb, RJ, Baker, T, Dube, B, Groves, DI, Hart, CJ and Gosselin, P. 2005. Distribution, character, and genesis of gold deposits in metamorphic terranes. *Economic Geology 100th Anniversary Volume*, pp. 407-450.

Gribnitz, KH. 1961. *Geological Notes on the Barberton Mountain Land*. Unpublished notes issued to delegates attending the 7th Commonwealth Mining and Metall. Congress.

Groves, DI. 1993. The crustal continuum model for late Archaean lode gold deposits of the Yilgarn Block, Western Australia. *Mineralium Deposita*, **28(6)**, pp. 366-374.

Groves, DI, and Foster, RP. 1991. Archean lode gold deposits. In RP Foster, (Eds), *Gold Metallogeny and exploration*, chapter 3, pp. 63–96. Blackie and son Ltd, London, 432 pages.

Groves, DI, Goldfarb, RJ, Gebre-Mariam, M, Hagemann, SG, and Robert, F, 1998. Orogenic gold deposits — a proposed classification in the context of their crustal distribution and relationship to other gold deposit types. Ore *Geology Reviews* **13**, pp. 7–27.

Groves, DI, Goldfarb, RJ, Robert, F and Hart, CJ. 2003. Gold deposits in metamorphic belts: overview of current understanding, outstanding problems, future research, and exploration significance. *Economic Geology*, **98(1)**, pp. 1-29.

Haas, JL. 1971. The effect of salinity on the maximum thermal gradient of a hydrothermal system at hydrostatic pressure. *Economic Geology*, **66(6)**, pp. 940-946.

Hammond, NQ, Moore, JM, and Sheets, RW. 2007. Physio-chemical conditions of ore-forming fluids associated with genesis of the Kalahari Goldridge deposit, Kraaipan Greenstone Belt, South Africa. *Ore Geology Reviews*, **30**, pp. 106–134.

Hayward, C.L., Reimold, W.U., Gibson, R.L. and Robb, L.J., (2005). Gold mineralization within the Witwatersrand Basin, South Africa: evidence for a modified placer origin, and the role of the Vredefort impact event. In: McDonald, I., Boyce, A.J., Butler, I.B., Herrington, R.J. & Polya, D.A., (eds). Mineral Deposits and Earth Evolution. Geological Society, London, Special Publications, 248:31–58.

Heinrich, CA. 2005. The physical and chemical evolution of low salinity magmatic fluids at the porphyry to epithermal transition: a thermodynamic study. *Mineralium Deposita*, **39(8)**, pp. 864-889.

Heinrich, CA, Driesner, T, Stefánsson, A and Seward, TM. (2004). Magmatic vapor contraction and the transport of gold from the porphyry environment to epithermal ore deposits. *Geology*, **32(9)**, pp. 761-764.

Hessler, AM and Lowe, DR. 2006. Weathering and sediment generation in the Archaean: An integrated study of the evolution of siliciclastic sedimentary rocks of the 3.2 Ga Moodies Group, Barberton Greenstone Belt, South Africa. *Precambrian Research*, **151**, pp. 185–210.

Heubeck, CE, Wendt JI, Toulkeridis T, Kroener A and Lowe, DR. 1993. Timing of deformation of the Archaean Barberton greenstone belt, South Africa: constraints from zircon dating of the Salisbury Kop Pluton. *South African Journal of Geology*, **96**, pp. 1-8.

Hofmann, A. 2005. The geochemistry of sedimentary rocks from the Fig Tree Group, Barberton greenstone belt: Implications for tectonic, hydrothermal and surface processes during mid-Archaean times. *Precambrian Research*, **143** (1-4), pp. 23–49.

Hofmann, A and Harris, C. 2008. Silica alteration zones in the Barberton greenstone belt: A window into sub-seafloor processes 3.5–3.3 Ga ago. *Chemical Geology*, **257**, pp. 221–239.

Hu, G, Dam-Johansen, K, Wedel, S and Hansen, JP. 2006. Decomposition and oxidation of pyrite. *Progress in Energy and Combustion Science*, **32**, pp. 295–314.

Kouzmanov, K and Pokrovski, GS. 2012. Hydrothermal controls on metal distribution in porphyry Cu (-Mo-Au) systems. *Special Publication of the Society of Economic Geologists*, **16(22)**, pp. 573-618.

Lana, C, Tohver E and Cawood, P. 2010. Quantifying rates of dome-and-keel formation in the Barberton granitoid-greenstone belt, South Africa. *Precambrian Research*, **177**, pp. 199–211.

Lana, C, Buick, I, Stevens, G, Rossouw, R, and De Wet, W. 2011. 3230-3200 Ma post-orogenic extension and mid-crustal magmatism along the south eastern margin of the Barberton Greenstone Belt, South Africa, *Journal of Structural Geology*, **33**, pp. 844-858.

Liebscher, A. 2010. Aqueous fluids at elevated pressure and temperature. *Geofluids*, **10(1-2)**, pp. 3-19.

Loucks, RR and Mavrogenes, JA. 1999. Gold solubility in supercritical hydrothermal brines measured in synthetic fluid inclusions. *Science*, **284(5423)**, pp. 2159-2163.

McCaffrey, KJW, Lonergan, L and Wilkinson, JJ. 1999. *Fractures, Fluid Flow and Mineralization.* Geological Society of London, Special Publications. 155 pages.

McLennan, SM, 1984. Petrological characteristics of Archaean greywackes. *Journal of Sedimentary Research*, **54** (**3)**, pp. 889-898.

Makovicky, E, Karup Møller, S, Makovicky, M and Rose Hansen, J. 1990. Experimental studies on the phase systems Fe Ni Pd S and Fe Pt Pd As S applied to PGE deposits. *Mineralogy and Petrology*, **42(1-4)**, pp. 307-319.

Markl, G and Bucher, K. 1998. Composition of fluids in the lower crust inferred from metamorphic salt in lower crustal rocks. *Nature*, **391(6669)**, pp. 781-783.

Merkle, R.K.W., Grote, W. and Graser, P., (2008). Compositional and textural peculiarities of gold-rich alloys from the Merensky Reef. S. A. Journal Geology, 111:177–186.

Micklethwaite, S and Cox, SF. 2004. Fault segment rupture, aftershock zone fluid flow, and mineralization. *Geology*, **32(9)**, pp. 813-816.

Mikucki, EJ. 1998. Hydrothermal transport and depositional processes in Archean lode gold systems: a review. *Ore Geology Reviews*, **13(1)**, pp. 307-321.

Miyashiro, A. 1973. *Metamorphism and Metamorphic belts*. George Allen and Unwin, London, 492.

Moisyenko, V and Mironyuk, A. 1998. Composition Peculiarities of Inclusions In Native Gold And Ore Quartz of The Russian Far East Deposits. Proceedings of the 30th International Geological Congress, Beijing, China, 4-14 August 1996. **9**, pp. 405-408.

Munyai, MR, Dirks, PHGM and Charlesworth, EG. 2011. Archaean gold mineralisation during post-orogenic extension in the New Consort gold mine, Barberton Greenstone Belt, South Africa. *South African Journal of Geology*, **114(2)**, pp. 121-144.

Ordonez-Calderon, JC, Polat, A, Fryer, BJ, Gagnon, JE, Raith, JG, and Appel, PWU. 2008. Evidence for HFSE and REE mobility during calc silicate metasomatism, Mesoarchaean (~3075 Ma) Ivisaartoq greenstone belt, southern West Greenland. *Precambrian Research*, **161**, pp. 317–340.

Otto, A, Dziggel, A, Kisters, AFM and Meyer, FM. 2007. The New Consort gold mine, Barberton greenstone belt, South Africa: orogenic gold mineralization in a condensed metamorphic profile. *Mineralium Deposita*, **42**, pp. 715–735.

Pan African Resources (2015). http://www.panafricanresources.com/operations-overview/barberton/ accessed on 2015-08-20.

Pearce, NJ, Perkins, WT, Westgate, JA, Gorton, MP, Jackson, SE, Neal, CR and Chenery, SP. 1997. A compilation of new and published major and trace element data for NIST SRM 610 and NIST SRM 612 glass reference materials. *Geostandards Newsletter*, **21(1)**, pp. 115-144.

Pettke, T., Diamond, LW, Kramers, JD. 1998. Mesothermal gold lodes in lodes in the north-western Alps: A review of genetic constraints from radiogenic isotopes, *European Journal of Mineral*, **12**, pp. 213-230.

Pettke, T, Frei, R, Kramers, JD and Villa, IM. 1997. Isotope systematics in vein gold from Brusson, Val d'Ayas (NW Italy) 3.(U+ Th) He and KAr in native Au and its fluid inclusions. *Chemical Geology*, **135(3)**, pp. 173-187.

Phillips, GN and Powell, R. 2009. Formation of gold deposits: Review and evaluation of the continuum model. *Earth Science Reviews*, **94(1)**, pp. 1-21.

Pokrovski, GS, Borisova, AY and Bychkov, AY. 2013. Speciation and transport of metals and metalloids in geological vapors. *Reviews in Mineralogy and Geochemistry*, **76(1)**, pp. 165-218.

Qian, G, Brugger, J, Skinner, WM, Chen, G, and Pring, A. 2010. An experimental study of the mechanism of the replacement of magnetite by pyrite up to 300 ^{0}C. *Geochimica et Cosmochimica Acta*, **74**, pp. 5610-5630.

Raymond, LA. 2002. *Petrology: The study of igneous, sedimentary and metamorphic rocks, 2ed*. McGraw-Hill Higher Education, Boston, MA.

Reich, M, Kesler, SE, Utsunomiya, S, Palenik, CS, Chryssoulis, SL and Ewing, RC. 2005. Solubility of gold in arsenian pyrite. *Geochima Cosmochima Acta*, **69**, pp. 2781–2796.

Saager, R and Koppel, V. 1976. Lead isotopes and trace elements from sulfides of Archean greenstone belts in South Africa; a contribution to the knowledge of the oldest known mineralizations. *Econ. Geol*. **71**, pp. 44–57.

Saha, I, and Venkatesh, AS. 2002. Invisible gold within sulphides from the Archaean Hutti-Maski schist belt, Southern India. *Journal of Asian Earth Sciences*, **20**, pp. 449-457.

Sanborn, M. and Telmer, K. (2003). The spatial resolution of LA-ICP-MS line scans across heterogeneous materials such as fish otoliths and zoned minerals. Journal of Analytical Atomic Spectrometry, 18:1231–1237.

Schouwstra, RP. 1985. *Kontroles van goudmineralisasie by die Sheba-goudmyn, Barberton-distrik* (PhD (Geology)). [Unpublished]: University of Johannesburg.

Schweigart, H and Liebenberg, WR. 1966. *Mineralogy and chemical behaviour of some refractory gold ores from the Barberton Mountain Land*. National Institute for Metallurgy Report (unpublished), 96 pages.

Semenko VA. 1990 The experience in use of the electron microscopy to study the fluid inclusions in native gold. *15th General Meeting of IMA, Beijing, China, Abstracts*, **vol. 11**, pp.72 75

Sibson, RH. 1987. Earthquake rupturing as a mineralizing agent in hydrothermal systems. *Geology*, **15(8)**, pp. 701-704.

Sibson, RH, Moore, JMM and Rankin, AH. 1975. Seismic pumping—a hydrothermal fluid transport mechanism. Journal of the Geological Society, **131(6**), pp. 653-659.

Simmons, SF, White, NC and John, DA. 2005. Geological characteristics of epithermal precious and base metal deposits. *Economic Geology 100th anniversary volume*, 29, 485 522.

Steele, TW and Carlton, CJ. 1961. Spectrographic Analysis of Samples of Pyritic Ore and Free Gold. G.M.O. Project No. 69/61, Government Metallurgical Laboratory, Johannesburg.

Steyn, M van R. 1976. *Die stratigraphie, die struktuur en die mineralisasie van die Fairview-myngebied, Distrik Barberton, Oos-Transvaal*. DSc thesis (unpublished), University of Pretoria, 184 pages.

Stiegler, MT, Lowe, DR, and Byerly, GR. 2010. The Petrogenesis of Volcaniclastic Komatiites in the Barberton Greenstone Belt, South Africa: a textural and Geochemical Study. *Journal of Petrology*, **51**, pp. 947-972.

Thébaud, N., Philippot, P., Rey, P., Brugger, J., Van Kranendonk, M , and Grassineau, N. 2008. Protracted fluid–rock interaction in the Mesoarchaean and implication for gold mineralization: Example from the Warrawoona syncline (Pilbara, Western Australia). *Earth and Planetary Science Letters*, **272**, pp. 639–655.

Tomkinson, MJ, and Lombard, A. 1990. Structure, metamorphism, and mineralisation in New Consort Gold Mines, Barberton greenstone belt, South Africa. In: Glover, JE, Ho, SE (Eds), *Abstract 3rd International Archaean Symposium*, University of western Australia, Australia, pp. 377-379.

Trommsdorff, V and Skippen, G. 1986. Vapour loss ("boiling") as a mechanism for fluid evolution in metamorphic rocks. *Contributions to Mineralogy and Petrology*, **94(3)**, pp. 317-322.

Trommsdorff, V, Skippen, G and Ulmer, P. 1985. Halite and sylvite as solid inclusions in high-grade metamorphic rocks. *Contributions to Mineralogy and Petrology*, **89(1)**, pp. 24-29.

van Hees, EH, Graney, JR and Kesler, SE. 1992. Fluid inclusions in native metals: II. Interpretation and implications. Pan-American Conference on Research on Fluid Inclusions, PACROFI IV, Los Angeles, 82

Van Kranendonk, MJ. 2011. Cool greenstone drips and the role of partial convective overturn in Barberton greenstone belt evolution. *Journal of African Earth Sciences*, **60**, pp. 346–352.

van Kranendonk, MJ, Kröner, A, Hegner, E and Connelly, J. 2009. Age, lithology and structural evolution of the c. 3.53 Ga Theespruit Formation in the Tjakastad area, southwestern Barberton Greenstone Belt, South Africa, with implications for Archaean tectonics. *Chemical Geology*, **261,** pp. 115–139.

Vanko, DA. 1986. High-chlorine amphiboles from oceanic rocks: product of highly-saline hydrothermal fluids?, American Mineralogist, **71**, pp. 51-59.

Vaughan, JP, and Kyin, A. 2004. Refractory gold ores in Archaean greenstones, Western Australia: mineralogy, gold paragenesis, metallurgical characterization and classification. Mineralogical Magazine, *Mineralogical Society of Great Britain and Ireland*. Vol. **68**; no. **2**, pp. 255-277.

Ward, JHW. 1995. Geology and metallogeny of the Barberton greenstone belt: a survey. *Journal of Africa Earth Sciences*, **21**, pp. 213-240.

Ward, JHW. 1999. The metallogeny of the Barberton Greenstone Belt, South Africa and Swaziland. *Geological Survey of South Africa, Memoir*, **86**, 116 pages.

Ward, JHW & Wilson, MGC (1998). Gold outside the Witwatersrand Basin. *In* The mineral resources of South Africa (MGC Wilson and CR Anhaeusser, eds): Handbook, Council for Geoscience, **16**, 350-386.

Warren, HV and Thompson, RM. 1944. Minor Elements in Gold. *Econ. Geol*., **39(7),** pp. 457-471.

Weatherley, DK and Henley, RW. 2013. Flash vaporization during earthquakes evidenced by gold deposits. Nature Geoscience, **6(4)**, pp. 294-298.

Wiggett, BSA, Brink, WCJ and Vorster, MA. 1986. *The Fairview gold mine, Barberton greenstone belt*. In: Mineral deposits of southern Africa, **1**, pp. 169-179.

Wilkinson, JJ. 2001. Fluid inclusions in hydrothermal ore deposits. *Lithos*, **55**, pp. 229-272.

Winderbaum, L, Ciobanu CL, Cook, NJ, Paul, M, Metcalfe, A and Gilbert, S. 2012. Multivariate Analysis of an LA-ICP-MS Trace Element Dataset for Pyrite. *International Association for Mathematical Geosciences*, **44**, pp. 823–842. DOI 10.1007/s11004-012-9418-1.

Yermolayev, PP, Bernard, VV and Khoroshilov, VL. 1993. Solid Microinclusions of Chlorides in Gold Bearing Metasomatites. *International Geology Review*, **35(5)**, pp. 485-492.

Zaikin, ID and Moiseyenko, VG. 1987. Kinetics of gas-release from gas-liquid inclusions in native metals. Transactions - *Doklady, Russian Academy of Sciences: Earth Science Section*, **292**, pp. 713-715.